Universidad de Valladolid

FACULTAD DE CIENCIAS

TRABAJO FIN DE GRADO

Grado en Química

A new plastic crystal composition with thermal energy storage potential

Autora: María Paz Cosgaya

Tutores: Julian Walker, José Miguel Martín Álvarez

Año 2023

Preface

I want to thank my supervisor in NTNU, Julian Walker, for letting me work with him during my stay in Norway and teaching me new ways of working in the lab. I want to also thank my supervisor in Valladolid, José Miguel Martín Álvarez, for assisting me during this year and agreeing on helping me with my thesis. It has been a pleasure to write my thesis with you both.

I also want to thank my family and friends, who supported me a lot, and the new friends that I made during my Erasmus. I really loved this year with you guys, and I hope we see each other soon.

Thank you all!

Abstract

Plastic crystals are supramolecular materials with a long-range crystallographic order that go through a phase transition to a phase where the crystal structure is maintained but a local structural disorder is introduced. This phase transition is a mesophase transition, and it is a solid-solid transition where the molecules gain enough free energy so they can rotate freely but there are still weak interactions that maintain the crystal structure. Due to this higher entropy change, these types of compounds can store more energy than other solid-solid state materials.

Bis-[(3,4-dimethylphenyl)oxonium](dibromo dichloro zincate) ($(DMP)_2$ $[ZnBr_2Cl_2]$) is a new composition with thermal energy storage potential that has been synthetized by in this project, with the aim of identifying new plastic crystal compositions. As the structure of the material was unknown, it was determined with X-ray diffraction, and the thermal properties of the material were studied using differential scanning calorimetry, so the different phase transitions of the material and its properties could be determined and decide whether or not the material is a plastic crystal. The results showed that small modifications of the synthesis change the crystal habit and properties of the final crystals. The DSC analyses showed that the material has a phase transition in a temperature range below 100 ºC that might be applicable to domestic (personal housing) applications, rather than industrial applications.

Resumen

Los cristales plásticos son unos materiales supramoleculares con un gran orden cristalográfico que tienen transiciones de fase a fases donde la estructura cristalina se mantiene, pero aparece un desorden estructural local. Esta transición de fase es conocida como la transición de mesofase, y es una transición sólido-sólido donde las moléculas ganan suficiente energía libre, por lo que pueden rotar libremente, pero aún mantienen interacciones débiles que mantienen la estructura cristalina. Estos compuestos tienen un mayor cambio de entropía en la transición a la mesofase que otros materiales con transiciones de fase sólido-sólido, con lo que pueden almacenar más energía.

Bis-[(3,4-dimetilfenil)oxonio](dibromo dicloro zincato) ($(DMP)_2$ $[ZnBr_2Cl_2]$) es un nuevo material con potencial de almacenamiento de energía térmica. Este compuesto ha sido sintetizado en este proyecto con el objetivo de identificar nuevas composiciones de cristales plásticos. La estructura de este material era desconocida, así que ha sido determinada por difracción de rayos X, y las propiedades térmicas del material han sido estudiadas utilizando calorimetría diferencial de barrido (DSC), para poder determinar las diferentes transiciones de fase del material y sus propiedades para poder determinar si es un cristal plástico o no. Los resultados del proyecto demostraron que pequeñas modificaciones del método de síntesis pueden cambiar el hábito cristalino y las propiedades de los cristales obtenidos. Los análisis de DSC mostraron que el material tiene una transición de fase en un rango de temperaturas menor de 100 ºC que puede ser usado para aplicaciones domésticas (vivienda personal), en lugar de aplicaciones industriales.

Contents

List of abbreviations

Phase Change Materials (PCMs)

Thermal Energy Storage (TES)

Plastic Crystals (PCs)

X-ray diffraction (XRD)

Organic PCMs (OPCMs)

Inorganic PCMs (IOPCMs)

Room temperature (RT)

Goodness of fit (Gof)

Bis-[(3,4-dimethylphenyl)oxonium](dibromo dichloro zincate) ($(DMP)_2$ $[ZnBr_2Cl_2]$)

1 Background

1.1 Motivation

In order to maximize the use of renewable energy sources that provide electricity intermittently rather than on demand, thermal energy storage (TES) is a crucial component of Europe's energy future. Additionally, it enables us to recover extra heat that would otherwise be lost through industrial processes or from the sun (solar thermal). The integration of renewable energy into our energy systems may thus be boosted, and CO_2 emissions can be decreased, with the help of TES. [1]

Based on how they store thermal energy, thermal energy storage materials can be classified into three groups, which are chemical heat, sensible heat, and latent heat storage.

Comparing these mentioned types of thermal energy storage systems, a promising technology for future development is latent heat storage, because of its potential for space optimization and efficiency. Furthermore, many thermal storage systems use toxic materials, but latent heat TES systems can be based on solid-state PCMs which are safer and could replace dangerous compounds for less toxic and environmentally friendly ones. [2]

According to their composition, PCMs can be classified into three groups: organic (for example paraffins, fatty acids and alcohols), inorganic (salt hydrates and metallic compounds), and eutectic (combination of organic-organic, inorganic-inorganic, and organic-inorganic PCMs). There is not much information about the last type, and organic PCMs are preferred over the inorganic ones because they have more advantages and less disadvantages, for instance, low volume changes, compatible with conventional construction materials, large working temperature range, recyclable and low cost. Some disadvantages are that they are flammable and have low thermal conductivity.

Due to their chemical composition and crystal structure, the properties of PCMs can change, rendering different materials more suitable to different temperature ranges and others altogether unsuitable for energy storage purposes. Some of the desired properties are: [3]

a) Phase transition temperatures that fit in the desired temperature range. There are three distinct low temperature range categories: up to 15 ºC for cooling application, 15-90 ºC for thermal comfort and above 90 ºC for hot water applications.
b) High density to occupy less volume and increase thermal energy stored.

c) High thermal conductivity, so that only minor temperature differences are required for charge and discharge the energy storage.
d) Non-toxicity.
e) Small volume change during in phase transitions.
f) Chemical stability.
g) Low cost.

A subclass of PCMs are plastic crystals (PCs), which were first categorized by Timmermans in 1935. These are supramolecular materials that possess a solid-mesophase transition before melting. The mesophase is a crystalline phase with long range structural order and a local molecular orientational disorder that is associated with a large entropy change; hence they are good phase change materials and interesting for TES and other applications. [4,5]

The search for new PC materials is ongoing and of interest for thermal energy technologies, for finding more accessible compounds with better thermophysical properties, i.e., enthalpy of transition, temperature of transition, thermal conductivity, thermal stability, and basic mechanical properties. Also, for substituting toxic and polluting compounds employed in energy storage applications.

1.2 Aim of work

The project's aim is to evaluate a potentially new phase change material, $(DMP)_2$ $[ZnBr_2Cl_2]$, and its potential use for TES. It is composed by an organic cation, [(3,4-dimethylphenyl)oxonium]$^+$ which has been protonated with H^+ from a HCl solution, and an inorganic anion $ZnBr_2Cl_2^{2-}$ that is produced from the dissolution of $ZnBr_2{\cdot}2H_2O$ and combination with dissolved Cl^-. As the organic components have similar characteristics as other plastic crystal materials, that is, they are small and globular in shape, which was identified by Timmermans et al. as a prerequisite for plastic crystals, it is expected that it may behave similarly. However, the different combination of fragments and specific structural symmetry may provide additional influences on the thermal properties. Since there is no known literature report of this material, the present work will develop a synthesis pathway and characterize the basic crystal structure and thermodynamic properties of the material. X-ray diffraction (XRD) and differential scanning calorimetry (DSC) were employed to determine the lattice parameters of the compound and calculate the total entropy and enthalpy change of the compound's transitions.

2 Introduction

This project deals with the synthesis and characterization of DMPBrClZn a material that is thought to be a plastic crystal. To familiarize the reader with the topic, the introduction will cover relevant topics: Latent heat and solid-state PCMs for TES, plastic crystals, crystallization from saturated solutions and thermodynamics of phase transitions.

2.1 Latent heat and solid-state phase change materials for thermal energy storage

Based on how they store energy, TES systems can be classified into three different types:
Thermochemical heat storage systems absorb or release energy due to the formation and breaking of chemical bonds, due to endothermic and exothermic chemical reactions.
Sensible heat storage systems work by the materials change in temperature, and thus their change in heat capacity or enthalpy as a function of temperature. These materials are usually "simple" materials such as rock and water and do not involve any change of state or phase transition during operation. They are typically characterized by their linear relationship of heat capacity with temperature and can be used for short and long-term storage. It is applicable to domestic systems but requires large volumes due to its low energy density. [6]
Latent heat storage systems store energy when a phase transition takes place at a desired temperature and provides a better density of energy storage. The energy density is the total amount of energy in a system per unit volume. The materials used for these systems are phase change materials (PCMs) and the transitions that can occur are liquid-gas, solid-liquid or solid-solid. The most used PCMs have solid-liquid transitions because the molecules in liquid state have more freedom of movement and, therefore, they have high energy change when melting of the solid takes place. Liquid-gas transitions also involve a high increase in energy of the molecules or atoms, but gas phases have much lower density compared to solid-liquid transitions, so the energy storage density is less. The solid-liquid PCMs however, have low thermal conductivity and challenges with large volume changes during melting and liquid leakage. As a result, PCMs with solid-solid phase transitions are increasingly becoming a promising choice, as they can possess high energy densities while avoiding the problems of liquid or gas leakage. Solid-solid PCMs have potential for high thermal energy storage capacity with minimum volume changes, so storage devices can be lighter and smaller. In addition, they

absorb and release latent heat at a constant temperature during the phase transition, which minimizes heat loss. [3,7]

PCMs are materials that use latent heat during the phase transitions to control temperatures within a specific range. The melting and solidification temperatures are critical parameters for PCMs for different applications, such as in the construction, biomedical, electronic and textile industries. Based on the temperature ranges in which the phase transition of these materials takes place, they can be divided into three groups: **low temperature PCMs**, when the transition occurs below 15 ºC, **mid temperature PCMs**, when the transition occurs between 15 and 90 ºC, and **high temperature PCMs**, when the transition occurs above 90 ºC. The most used PCMs are those in the mid temperature range, because they can be applied in energy-savings in building construction and in medical industry, among others. [8]

PCMs can also be classified according to the phase transitions they go through, such as liquid-gas, solid-liquid and solid-solid. Because of liquid-gas or solid-liquid constraints, solid-solid materials are preferable for specific applications such as building heating and cooling. These have smaller volume changes associated with the transition, which makes them economically and practically appealing as materials for TES systems, because the containers can be more practical and affordable to build. In addition, there is no risk of leakage or volatilization in these compounds. [9]

In solid-solid phase transitions, materials go through polymorphic phase transitions from solid state crystallographic phases to mesophases. These different phases of the same compound can possess diverse properties, such as ferroelectricity, superconductivity, magnetic ordering, etc. Usually, over the transition temperature, the material changes from an ordered phase to a relatively disordered one, so there is a large and reversible entropy change which permits PCMs to charge and discharge latent heat energy storage. [10]

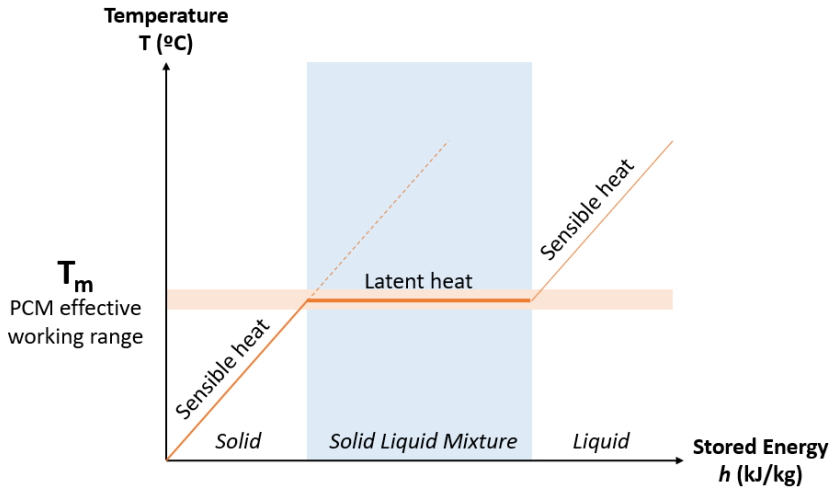

Figure 2.1. Representation of the storable heat energy in sensible and latent heat during phase transition. [9]

The material reaches its transition temperature during the charging phase of latent heat energy storage devices, resulting in an endothermic process in which the PCM stores a considerable quantity of thermal energy. In this state, the material is charged, and the energy is stored. When the temperature decreases and the material goes through a reverse transition often at lower temperature, the heat is released by an exothermic process, the discharging process, and the material returns to the initial phase. [11]

Some of the properties of these materials can be improved depending on the material nature of PCMs. Some of the advantages and disadvantages of organic PCMs (OPCMs) and inorganic PCMs (IOPCMs) are shown in the **Table 2.1.**

PCMs	Advantages	Disadvantages
OPCMs	Non corrosives	Low thermal conductivity
	Chemical and thermal stability	Flammable
	Good thermal stability	
	Large working temperature range	
	High heat of fusion	
IOPCMs	High thermal conductivity compared with OPCMs	Corrosive to metal
	Non-flammable	Phase separation
	High thermal conductivity	High volume changes

Table 2.1: Advantages and disadvantages of organic and inorganic PCMs.

There is also another type of PCMs which are eutectic or hybrid PCMs that are made by organic-organic, organic-inorganic and inorganic-inorganic, and by combining them it is possible to combine the stability and minor volume change of inorganics with the temperature range or operation of organics by mixing inorganic and organic fragments in the same structure. [12,13]

Family	Material	ΔH (J/g)
Organic	Pentaerythritol (PE)	300.00
	Pentaglycerin (PG)	170.70
	Neopentylglycol (NPG)	119.40
	Paraffin	200.00
Hybrid	bis-[(3,4-dimethylphenyl)oxonium](dibromo dichloro zincate) ($(DMP)_2$ $[ZnBr_2Cl_2]$)	~120.00
	$[(CH_3)_4N][FeBrCl_3]$ (TMA FBC)	19.00
	$[(C_2H_5)_4N][FeBrCl_3]$ (TEA FBC)	65.70
Inorganic	FE-15CO	52.00
	$CaBr_2 \cdot 6H_2O$	115.50

Table 2.2: Comparison of different PCM materials showing their enthalpies.

2.2 Plastic crystals

Plastic crystals (PCs) are materials that were first categorized by Timmermans in 1938 and they have been studied since then. He defined them as materials formed of globular organic molecules that are ordered according to a cubic symmetry and present well determined thermal stability between the solid and liquid state [14], however, other crystalline systems have been seen in this type of materials. They are a subcategory of PCMs and are materials with long-range crystallographic order and local structural disorder, which gives them unique features. Since they are crystals, they are ordered and there is a crystal lattice that is extended periodically over three directions in a real space. The motif is the building block that repeats itself in the crystal lattice, and any atoms can constitute it, occupying different space positions that are orderly repeated. [15] They are compounds composed of small molecules with globular structures. [16,17]

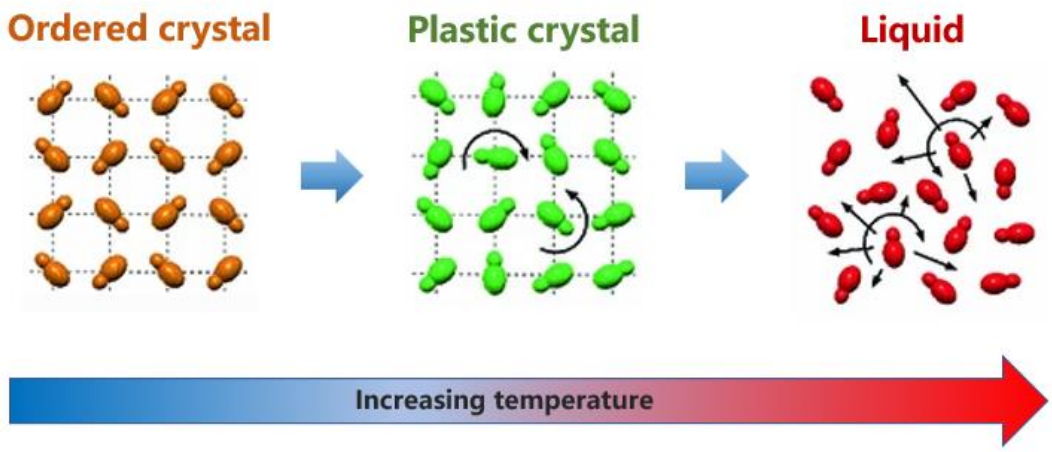

Figure 2.2: Scheme of phase transitions activated with temperature. The ordered crystal gains rotational freedom and becomes a plastic crystal, where the mass centers of the molecules are fixed in a lattice, giving long range order, before finally the intermolecular bonding is dissolved, and the material become a liquid. [18]

This is the reason why PCs are suitable materials for thermal energy storage because there is a high entropy change that allows storing thermal energy while maintaining some properties of solid-state materials. Therefore, the challenges that arise during the transition from solid to liquid or gas, such as leakage, are not present in solid-state materials, so it is safer to manage and use.

To determine if materials are potential plastic crystals, Timmermans proposed one simple criterion: if the ratio between the distance separating the centers of two adjacent molecules and the maximum diameter of a molecule is greater than 0.81, then the existence of plastic crystals is probable at a certain temperature range.

In the plastic crystal phase, the molecules occupy an almost spherical space, which allows dense cubic packing. For this reason, cubic symmetry is common during the plastic crystal phase. And as globular molecules occupy more space than expected in an ordered crystalline phase, there are weaker interactions between units, so less energy is required for breaking the chemical bonds and there is a high plasticity. [19]

There are plastic ionic plastic crystals composed of inorganic anions bonded to organic cations. When they contain only one organic species, they have low entropy change in the melting transition, however if there are two different organic species, the entropy will be higher. This is because the rotational contribution of the entropy of fusion is already in the solid state. The organic cations have weak chemical bonds that lead to higher transition entropies, while

inorganic components boost thermal stability. In addition, they have chemical flexibility that permits to adjust some parameters, such as transition temperature or conductivity, by introducing selective impurities to the material. [20,21]

This possibility of modifying the transition temperatures is one of the goals for development of new materials, to improve their performance and to develop more efficient systems. In addition, it depends on the type of applications wanted of these kinds of materials, because if they are used for building applications, the temperatures range should be a low one, for maximizing comfort.

2.3 Crystallization

Crystallization is the internal ordination of atoms or molecules of a liquid or gas solution to a crystal. The final crystal depends on several factors such as pressure, temperature, etc. It is a natural process that occurs in two steps: nucleation and growth. As the plastic crystal of this project is synthetized by crystallization from a solution it is necessary to discuss the theory of crystal nucleation and growth.

2.3.1 Nucleation

Nucleation is the formation of small solid particles and there are two types:

Homogeneous nucleation occurs in pure systems and is the uniform formation of the new phase, and this formation is associated with the transformation of the phase. It is expected to observe solidification below the melting temperature due to the associated energy with the solid crystalline structure, which is lower than the liquid's energy. The energy difference between phases is the free energy per unit of volume and is the driving force behind the solidification. It depends on the volume of the particle and temperature, and there will only be spontaneous nucleation in homogeneous systems when this free energy has a negative value. [22]

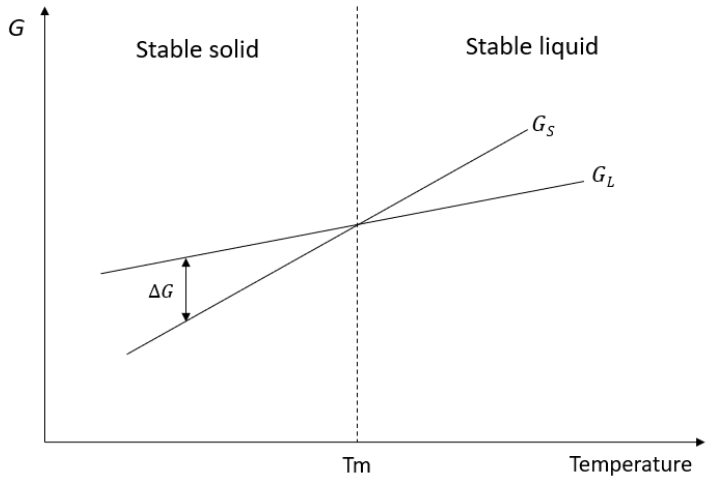

Figure 2.3: The different phases are stable depending on the temperature. If it is below the solidification temperature, the solid state will be more stable than the liquid one because the energy required in the solid phase will be less. On the contrary, if the temperature is higher, the stable phase will be the liquid one, because in this case its energy is the lowest and is more spontaneous.

When there are two phases coexisting, a solid-liquid interface is formed and there is an associated free surface energy, σ, a positive energy unfavorable to the solid formation. Considering this factor, the total ΔG would be:

$$\Delta G = \Delta G_v + \Delta G_s \quad \textbf{(2.1)}$$

$$\Delta G = \frac{4}{3}\pi r^3 \Delta G + 4\pi r^2 \sigma \quad \textbf{(2.2)}$$

where ΔG_v is the volume of the spheric particle per ΔG and has a negative value, and ΔG_s is the spheric surface per surface energy (σ).

An embryo is a small solid particle that is formed from the liquid solution when the atoms agglomerate and is unstable and it may grow or not depending on the conditions. [22]

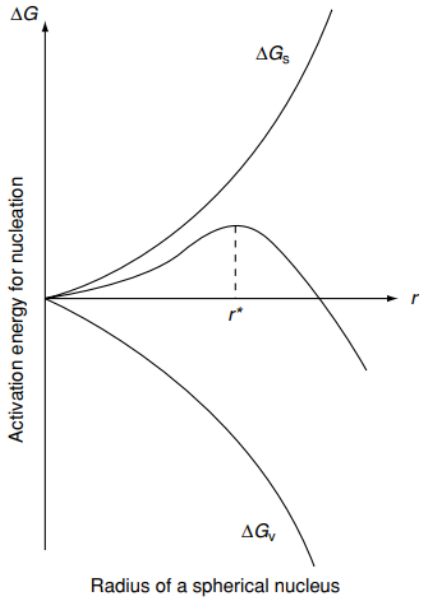

Figure 2.4: The dependence of the two energy contributions, ΔG_v and ΔG_s on r, the crystal size, shows the critical change in free energy, which, as a sort of activation energy, is the energy that must be overcome for the nucleus to be able to expand. [23]

At first, ΔG_s contributes more to free energy than ΔG_v, and if the particle has a higher radius than the critical radius, r^*, this will continue growing while the energy decreases and a nucleus is formed and will keep growing. If the size of the radius is lower than critical one, the embryo will redissolve and disappear because that is the most stable option. The formation of the embryos is a statistic process because lots of them are formed and redissolved. A posterior growth makes the total free energy to decrease only if by any chance an embryo with a higher radius than the critical one is formed.

The number of stable nuclei is temperature-dependent, therefore rising temperatures will result in higher activation free energies and fewer stable nuclei.

Since the system has a lower temperature than the melting one, it is considered subcooled. Subcooling is the difference between the solidification temperature and the real system's temperature. Sometimes, when the material is too pure, a bigger subcooling is necessary for forming stable nuclei.

Heterogenous nucleation occurs when there are impurities in the system, and the critical radius is achieved when a spheric portion with the exact curvature of r^* is added. This type of nucleation is easier, because for achieving the critical radius, less subcooling is required and nucleation will occur faster. [22]

2.3.2 Growth

Growth is the incorporation of new molecules to the formed and stable nuclei to increase their size. There are two types of growth:

Planar growth occurs when there is a heterogeneous nucleation. At the solidification temperature, some liquid particles are incorporated into the solid surfaces and inside this solid phase, the temperature decreases when the distance to the melting temperature is greater, because it is more stable at lower temperatures. Inside the liquid phase, the temperature increases when the distance to the solidification temperature is greater because it is more stable at higher temperatures.

As the temperature increases, latent heat of fusion is released to the solid state, where the temperature is lower, for continuing growth. In the solid-liquid interface there is a protuberance and a flat surface. If the particle incorporates to the protuberance, the heat will be expanded to the interior in an angle lower than 180 º. If the particle joins to the flat surface, the heat spreads in a 180 º angle to the interior. This last situation is preferable because the heat can travel faster, and the protuberance will disappear. [22]

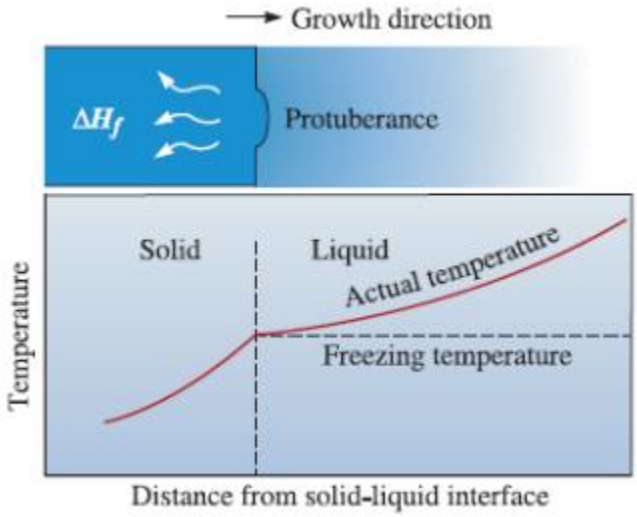

Figure 2.5: If the temperature is above the melting temperature, there will not be any protuberance and the flat surface will persist. [22]

Dendritic growth takes place in a homogeneous nucleation. At the melting temperature, liquid particles are incorporated into the solid's surface. Inside the solid state the temperature decreases when the difference between the temperature and the melting one is greater because it is stable at a less temperature. In the liquid state there will be a decrease in the temperature below the solidification point because there is subcooling, and then it increases as usual.

If the nucleus grows, latent heat of fusion is released and will be directed to the coldest regions, but preferable the liquid one because absorbs heat better. There is also a protuberance and a flat surface. If a particle incorporates into the flat surface, the heat will be spread in a 180 º angle into the interior. However, if the particle joins the protuberance, the angle will be higher than 180 º and growth will be faster than in the other surface, and another protuberance will be formed and when it grows another will be created. The result of this process is a dendrite. [22]

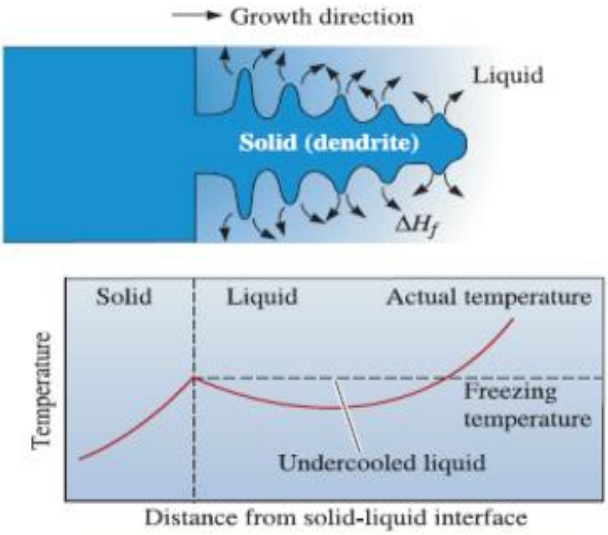

Figure 2.6: If the liquid is subcooled, a protuberance can grow into a dendrite faster. Latent heat of fusion will be released, and the liquid's temperature will increase to the solidification temperature. [22]

2.3.3 Crystal habit

The faces of a crystal are the crystal habit, and its development depends on several factors, such as environmental conditions and defects. There can be different variations in their growth, such as in one direction in a needle-shape, which is an acicular habit, or a slow-growing that produces a flat plate-like crystal, which is a tabular habit. Saturated solutions or supercooling can affect considerably the crystal habit and its growth control.

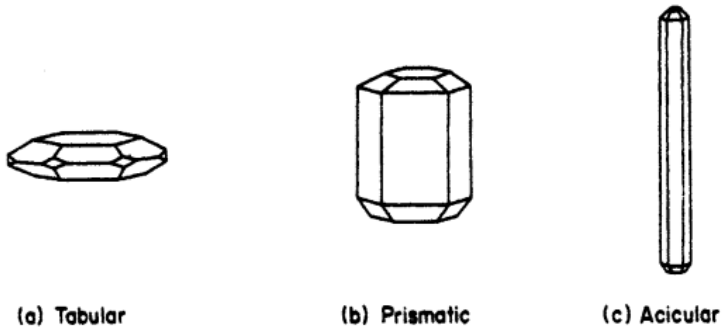

Figure 2.7: Different crystal habits of a hexagonal crystal.[24]

The most influential crystal faces are those with the lowest Miller indices and highest reticular densities. In order words, the faces with the greatest interplanar faces, d_{hkl} . In addition, due to the surface energy theories of crystal growth, the equilibrium form should be such that the crystal has the least amount of total surface free energy per unit volume. [24]

2.4 Thermodynamics of phase transitions

When a substance gains enough energy or pressure, a phase transition takes place and the material changes from one state to another, e. g. solid to liquid. However, materials can also undergo structural transitions while remaining in the solid state, this is known as a polymorphic phase transition. In these transitions, materials can lose or gain different properties such as superconductivity, ferromagnetism, or ferroelectricity. These transitions also have different thermodynamic characteristics depending on what type of structural changes are taking place. As a result, polymorphic phase transitions can be associated with a change in the materials latent heat, or not. By the Ehrenfest classification, first order transitions are the ones where the first derivative of a magnitude is discontinuous, and the second order transitions are the one that have a discontinuity in the second derivative. Heat capacity is a product of the second derivative of the Gibbs free energy. It is discontinuous for a second order transition and infinite at a first order transition. [25]

The search of new hybrid plastic crystal compositions involves finding combinations of organic and inorganic molecules. The inorganic molecules are mainly metal halide tetrahedra, including transition metals like Fe, Zn, Mn, and halides such as Cl, Br, I. In this project, it was interesting

to look at higher charged systems beyond the +1 and -1 charge ions. This was due to the fact that there had been less investigations on these systems, so the Zn-Halide$_4$ tetrahedra with a -2 charge was investigated. In combination with this, a polar globular cation was also investigated. The cyclic amine species fit this description. 3,4-dimethylphenol was chosen because it was commercially available and fit the description above.

For studying and determine the entropy and enthalpy of the transitions of the material, the equation **(2.3)** was used:

$$\Delta G = \Delta H - T\Delta S \qquad \textbf{(2.3)}$$

With DSC, the enthalpy is calculated, and it can be related thanks to the equation with the entropy and free energy. It is important to know the value of the entropy because it is what measures the storage capacity of the material.

2.5 Quenching

Rapidly cooling a substance to modify its mechanical properties is a process known as quenching. Quenching is typically done to give materials the desired mechanical qualities, such as improved strength and hardness. It is usually used among metallurgists, glass scientists and ceramicists, for developing microstructures and crystal structures and hence the desired properties in difference metals. For a quenching process, the material is heated to a temperature above its recrystallization temperature but below the melting point. Then, after keeping the material in this temperature for some time, it is quenched to room temperature or below. This practice has recently started to be used for retaining phase structures at high temperatures. [26] It has also been used in molecular crystals in their plastic phase for obtaining glasses of a new kind. These crystals are rapidly cooled for preventing the transition towards the low temperature ordered phase, and the disordered system goes into a glassy state. On gradual reheating, a "glass transition" takes place in which the glassy form, in which the orientational disorder is frozen, and is irreversibly transformed into the low temperature metastable form of the plastic phase. [27]

3 Experimental

3.1 Synthesis of $(DMP)_2$ $[ZnBr_2Cl_2]$

The synthesis of $(DMP)_2$ $[ZnBr_2Cl_2]$ was carried out in two ways in which the ratio of the reactants was varied.

It was first done three times with some small changes to the synthesis, however here the main method is presented and later on the differences will be explained.

Synthesis (illustrated in **Figure 3.1**) of the plastic crystal material was carried out using 3,4-dimetylphenol and $ZnBr_2 \cdot H_2O$ as precursors, and they were weighed out to achieve a 1:1 stoichiometric ratio. First, 1,757 g of the 3,4-dimethylphenol was weighed and then dissolved in 4 mL of ethanol. For protonation of the organic molecule to [3,4-dimethylphenol]H^+, 0.874 mL of HCl was added to the dissolved organic precursor and mixed for 12 hours with a magnetic stirrer at room temperature. During this process the liquid was allowed to evaporate as a means of dehydrating the material from any residual moisture in the starting precursor, and the product crystallized. Once the protonation was completed the product was redissolved with EtOH. Afterwards, 3,759 g of $ZnBr_2 \cdot H_2O$ were weighed and dissolved in 4 mL of ethanol. Then, the organic cation was mixed with the dissolved inorganic anion in the organic solvent for forty minutes and subsequently allowed to naturally cool to room temperature, crystallizing by evaporation of the solvent, without covering the beaker at any time.

The same synthetic route was performed two additional times with a different reactants ratio (**Figure 3.1**), but the amount of 3,4-dimethylphenol used was 2,3 g. 0,3 mL of HCl were used for the protonation of the organic compound, and the quantity of the inorganic compound, $ZnBr_2 \cdot H_2O$, was 2,1 g.

Materials	Chemical formula	Manufacturer	Purity (%)
3,4-dimethylphenol	$C_8H_{10}O$	Sigma-Aldrich	98
Zinc bromide dihydrate	$ZnBr_2 \cdot H_2O$	Sigma-Aldrich	99

Table 3.1: List of chemicals used in the synthesis.

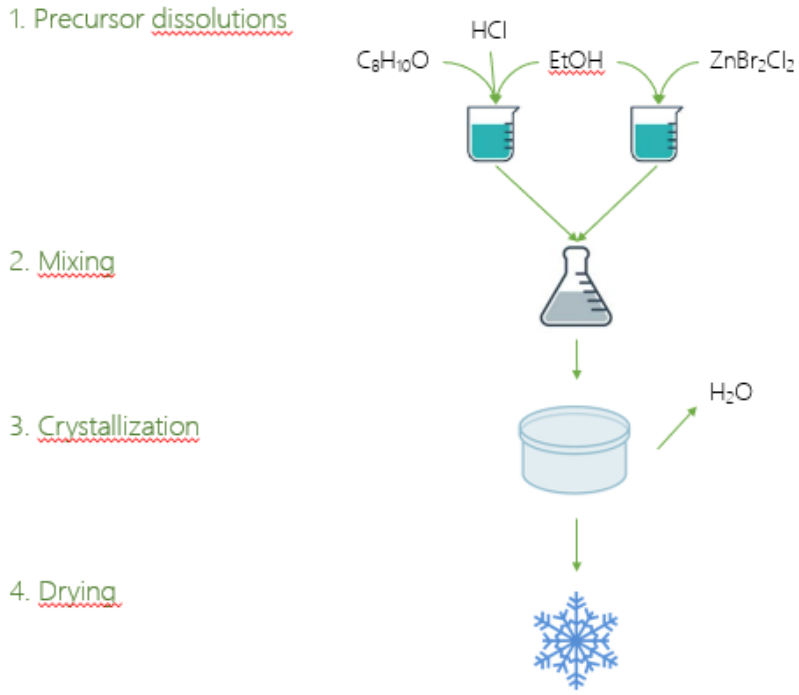

Figure 3.1: Synthesis route for the plastic crystal.

3.2 Structural determination

3.2.1 XRD

XRD analyses were performed to determine the crystal structure of the plastic crystal. The crystals were crushed in a mortar and then placed into a kapton holder. With a sliding glass, the surface of the sample was made smooth and flat. Once the sample holder was prepared, it was placed into the D8-Focus X-ray diffractometer with CuKα radiation ($\hbar\omega = 8.04$ keV, $\lambda = 1.5406$ Å). All samples were characterized from 5-55 degrees 2θ, for 30 minutes with 0.6º slit-opening.

The XRD data was then studied using DIFFRAC.SUITE TOPAS® software. First, a peak indexing of the analysis was done, and different crystal structures were studied. In each structure, several space groups were chosen according to their goodness of fit (Gof). The space groups with higher values of Gof fitted better with the material's structure. These space groups, their respective Gof and lattice parameters were noted.

Next, a Pawley fit was done with each of those space groups, and the better fits were the ones with the lowest Gof. (The change in the Gof from the highest to lowest being the better fit is an anomaly of the DIFFRAC.SUITE TOPAS® software). A new *hkl* phase was created every time

a new space group was studied. The lattice parameters that were determined during the initial peak indexing were introduced in the *hkl* phase structure as the starting parameters and were refined one by one. Each fit was performed independently in order to always start with the same background parameters. This was important to ensure the same starting point for each refinement and reproducibility of the fitting.

3.2.2 Raman spectroscopy

Raman spectroscopy is a non-destructive method of evaluation that gives details on the chemical structure, phase, and molecular interactions of a sample. It is based on how light interacts with molecular vibrations, phonons or other excitations in the system. [28]

This analysis was performed for studying the material's structure and checking if the samples suppressed under a thermal cycle changed, so the instability in their crystal system could be explained.

3.3 Thermodynamic characterization

3.3.1 DSC

DSC was used to observe the phase transitions as a function of temperature. In these analyses, an empty aluminum crucible and a closed lid were weighed, and then approximately 10 mg of $(DMP)_2$ $[ZnBr_2Cl_2]$ was added into the crucible. The crucible was closed with the lid using a pressing tool.

After weighing the mass of the reference crucible with lid and the sample mass was added to the software and the sample was placed in the Netzsch Polyma DSC 214.

Different thermal programs were used to observe different phenomena. In the first program two consecutive thermal cycles were run with a maximum temperature of 80 ºC and a minimum temperature of -20 ºC **(Figure 3.2**). The heating and cooling rate was 10 K/min and the holding time at the maximum temperature was 5 minutes. This was the standard program intended to examine the reversibility of the transitions occurring within this temperature range and calculate the enthalpy of the transition.

In addition, another run of two thermal cycles was done but with a minimum temperature of 20 ºC (**Figure 3.3**). This measurement was first conducted due to a malfunction in the cooling program but was actually used to reveal the sensitivity of the transition on set temperature on cooling. There were further temperature cycles conducted as well, with minimum temperatures

of -20°C and maximum temperatures of 80°C, which was executed five times, and another one with the same minimum temperature but with a maximum temperature that first was 75 ºC and it was increased every cycle 5 ºC until 100 ºC (**Figure 3.4**). Both these measurements were designed to study the degradation of the material by looking at the transition enthalpy reduction with each consecutive thermal cycle and with increasing maximum temperature respectively. In all the analyses the flow gases were synthetic air gas mixture (20 mL/min), nitrogen (40 mL/min), nitrogen as safety gas (60 mL/min) and liquid nitrogen for controlled cooling.

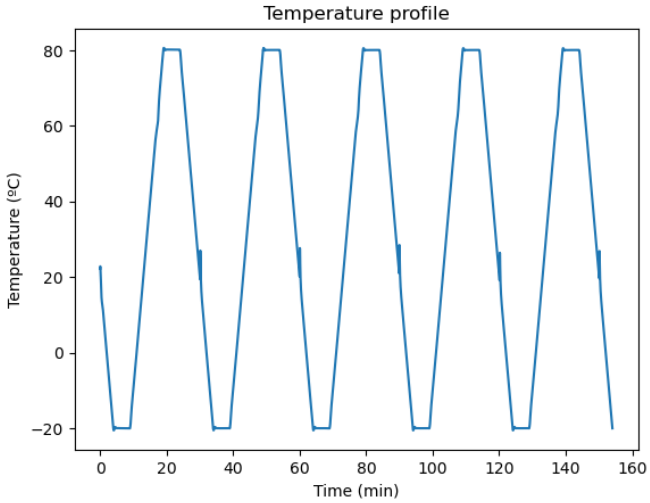

Figure 3.2: Thermal profile of the DSC analysis from -20 to 80 ºC.

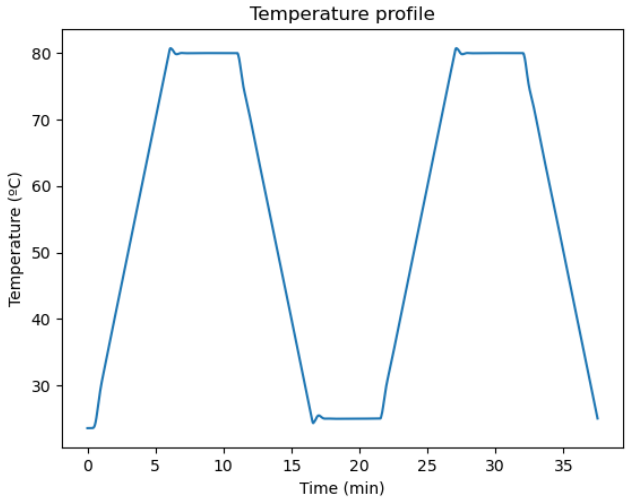

Figure 3.3: Thermal profile of the DSC analysis from 20 to 80 ºC.

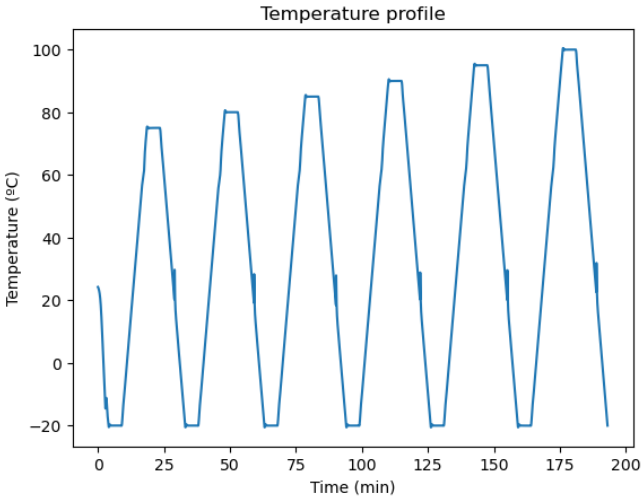

Figure 3.4: Thermal profile of the DSC analysis from -20 to 100 ºC.

4 Results

4.1 Sample clarification

These crystals have been synthetized a total of four times and each of these attempts is discussed in the following section. There were samples that were synthetized by previous students in June, and there have also been results from those crystals that are also discussed here. For clarifying, each of these samples named according to the table below.

Sample name	Description
June 2022 crystals*	Samples prepared by previous students in June 2022. The crystals were white.
Crystallization attempt 1	The first attempt to crystallizing these samples in October 2022. Instead of crystals, a gel was obtained.
Crystallization attempt 2	The second attempt to crystallizing these samples in late October 2022. The obtained crystals were shaped like long-needles in the walls of the beaker and there were brownish crystals at the bottom of the beaker.
Crystallization attempt 3	The tird attempt to crystallizing these samples in November 2022. The crystals were brownish and all of them crystallized at the bottom of the beaker.

Crystallization attempt 4	The fourth attempt to crystallizing the sample in March 2023. The crystals crystallized at the bottom of the beaker and were white, but after leaving them in a crystallizer for drying at room temperature by evaporation, they started to be pinkish and never dried completely
Crystallization attempt 5	The fifth attempt to crystallizing the sample in May 2023. It crystallized at the bottom of the beaker and was white. It was then dried with a Kitasato flask by doing a solid-liquid separation.

Table 4.1: Name and description of samples produced during this study.

*The samples with an asterisk were not crystallized by María Paz Cosgaya but by previous students. However, all data collection and data analyses of these samples as presented here was performed by María Paz Cosgaya.

Some differences were observed between the different crystal batches. The origin of which is currently not fully understood, however because of the differences, each batch is going to be discussed here.

4.2 Synthesis observations

4.2.1 June 2022 crystals

In June 2022, this material was synthetized by other students in the FACET group, and the obtained crystals were white colored. This synthesis was carried out using the same precursor mentioned in the Experimental section (3.1) but the dissolved 3,4-dimethylphenol in EtOH was protonated with HCl and left overnight at a 50 ºC reflux. Then, dissolved dihydrate zinc bromide was added, and the final solution crystallized by evaporation.

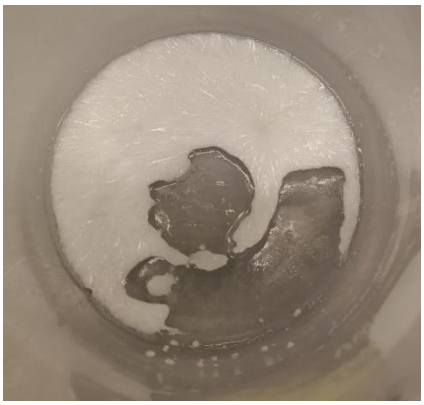

Figure 4.1: *June 2022 crystals* synthetized from the first synthesis by other students.

4.2.2 Crystallization attempt 1

These crystals were produced using the method described in the experimental section, with the first quantities, with the following differences: an aluminum foil that had holes in it was used on top, and the temperature of evaporation was 50 ºC. The final crystals were reddish instead of white, as in previous studies in the FACET group, and it did not dry completely. The aluminum foil was also found to be corroded after the crystallization attempt was concluded.

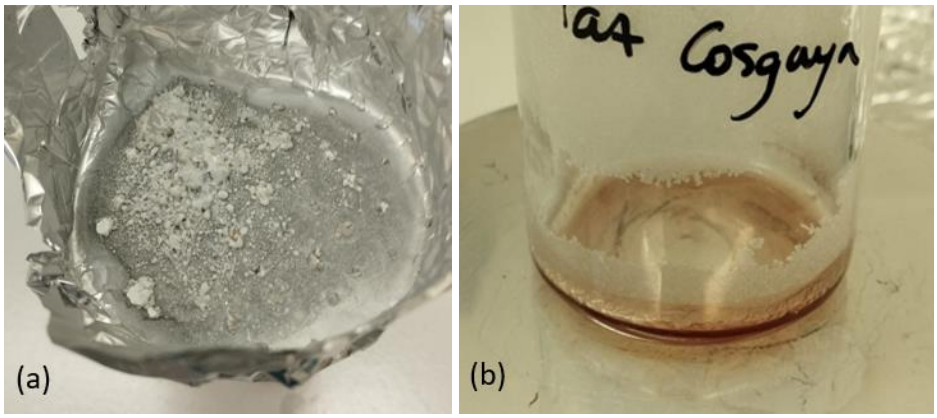

Figure 4.2: (a) Corroded aluminum foil and (b) contaminated final solution.

The final product was then put in a crystal container and dried in the vacuum oven at 50 ºC, so as to try to separate the crystals from the liquid and do an XRD analysis, but they melted, and the sample was unusable. The resulting sample became a gel rather than a crystalline product.

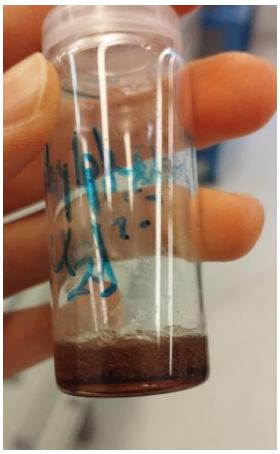

Figure 4.3: Sample remaining after *Crystallization attempt 1*. Sample formed a brown gel rather thana crystalline solid.

4.2.3 Crystallization attempt 2

In the second attempt, the method described in the experimental section was followed but with the following differences: the beaker with the solution was covered with parafilm that had holes in it and it the temperature of heating while evaporating was 50 ºC. The solution crystallized, but with very different crystal habits to that observed by the previous students. The product crystallized on the walls of the beaker indicating that solvent evaporation, and consequently crystallization, occurred too fast. These crystals had a long-needle shape and were white, but there were some brownish crystals at the bottom of the beaker.

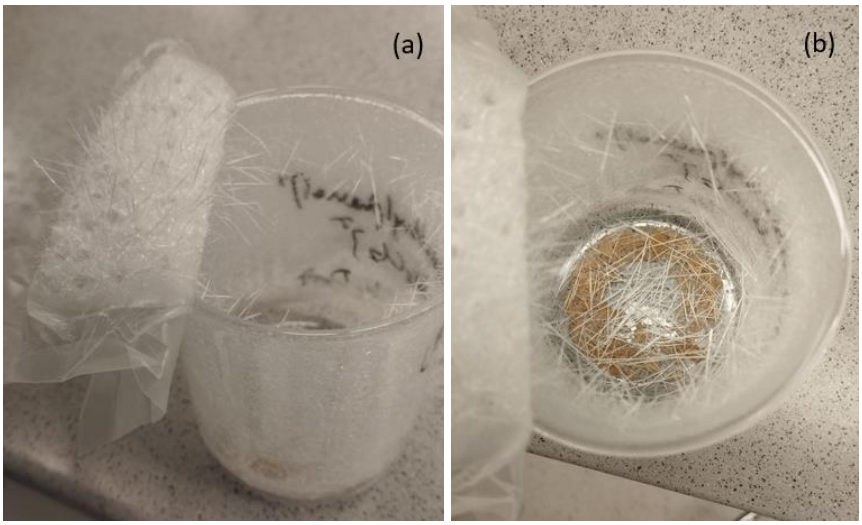

Figure 4.4: (a) Long-needle shape crystals and (b) brownish crystals at the bottom of the beaker.

These crystals were separated for making XRD analyses. The results of these will be shown in the XRD section 4.3.

4.2.4 Crystallization attempt 3

The third synthesis was where the method explained in the experimental section with the first quantities was followed without any differences.

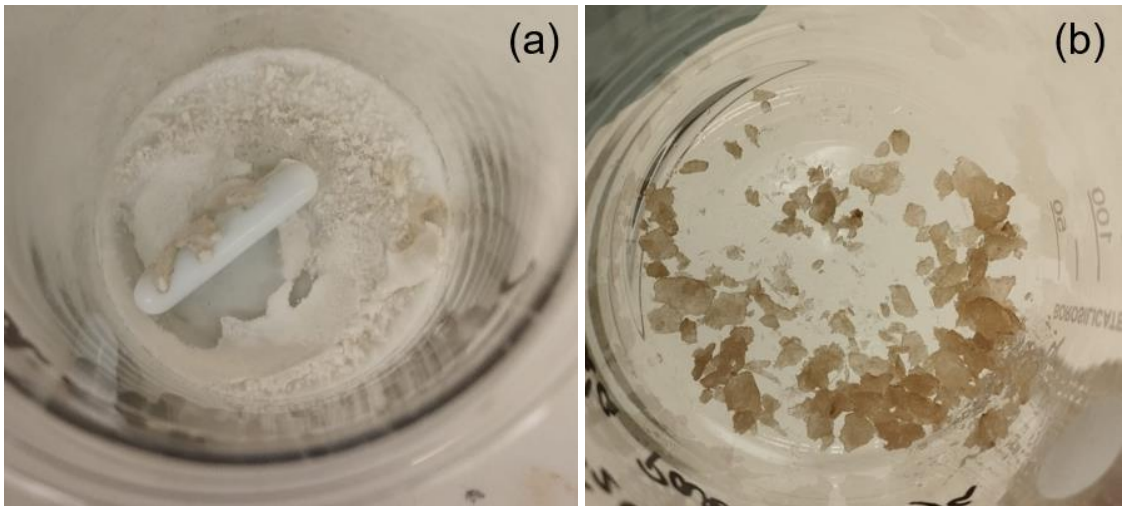

Figure 4.5: (a) Organic compound with HCl after protonation and evaporation of EtOH and (b) final agglomerated crystals.

The final crystals were hard to completely dry, so they were left in a watch glass inside a fume hood for several days. However, the crystals did still have some variations in color indicating some difference compared to those made in June.

4.2.5 Crystallization attempt 4

The fourth synthesis was carried out following the experimental method with the second quantities of each reagent. White crystals formed at the bottom of the beaker but did not entirely dry up through evaporation at ambient temperature. They were put in a crystallizer so they could dry out more quickly, and they began to change color to a pinkish one like in earlier syntheses.

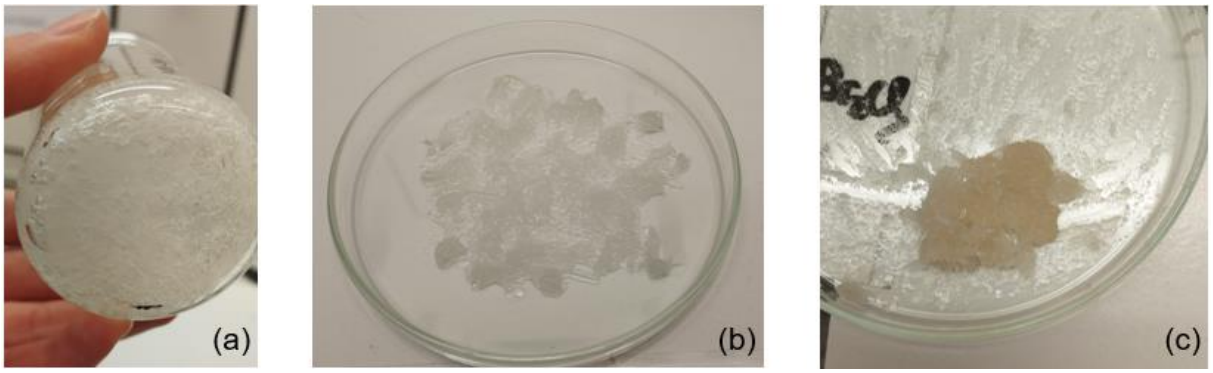

Figure 4.6: (a) White crystals at the bottom of the beaker. (b) Crystals placed in a crystallizer for drying. (c) Pinkish crystals, still wet.

4.2.6 Crystallization attempt 5

In the fifth crystallization the crystals crystallized at the bottom of the beaker and were also white, like in *Crystallization attempt 4*. They were still wet, so they were dried with a Kitasato flask, and the color did not change the color during the drying process.

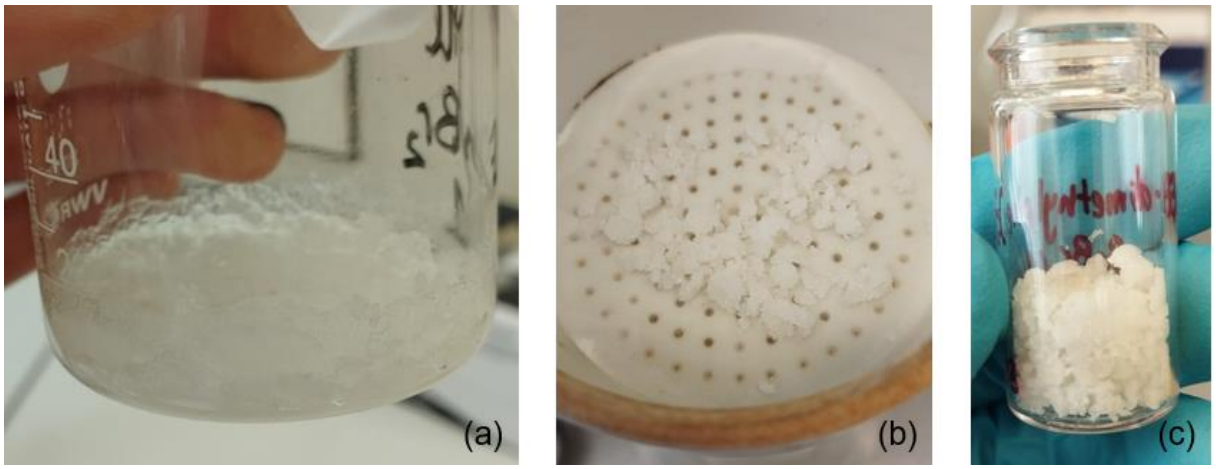

Figure 4.7: (a) White crystals at the bottom of the beaker. (b) Drying with Kitasato flask. (c) Dried crystals in a vial.

4.3 Crystal structure

The crystal structure of the plastic crystal was determined by XRD. The determination of its structure was done using the X-ray powder diffractogram from the *June 2022 crystals* and then compared with more XRD analyses from the samples synthetized this semester.

4.3.1 June 2022 crystals

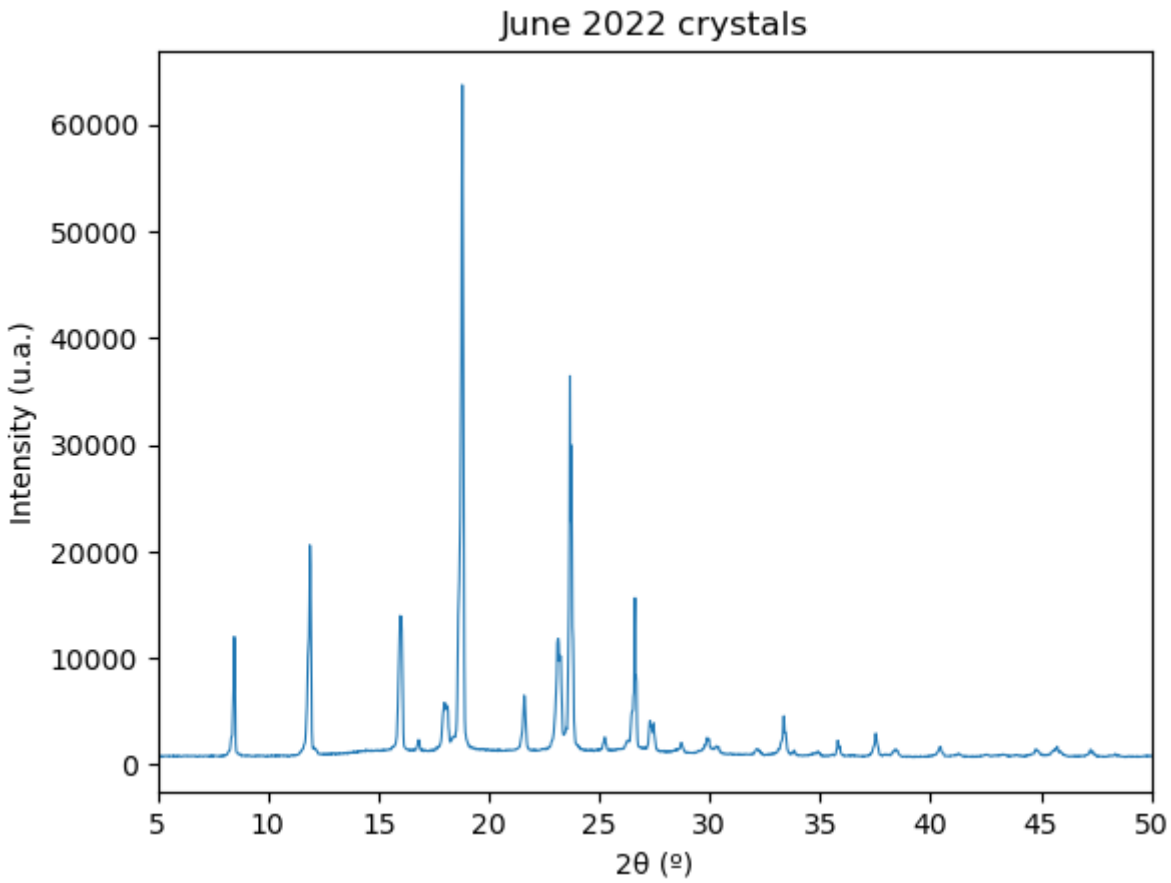

Figure 4.8: Diffractogram of the *June 2022 crystals* done in this semester. Note: The Miller indices of the Bragg diffraction peaks are not labelled in this thesis until after the crystal structure identification process has been discussed, in order to highlight that the crystal structure was initially unknown.

4.3.2 Determination of the crystal structure

The crystal structure of the material is unknown, and no references were found about it, so in this specialization project the determination of the crystal system, the space group symmetry and the lattice parameters were attempted. For the characterization of the structure, the data from the diffractogram showed in the **Figure 4.8** was used, which was obtained from the *June 2022 crystals*.

The data was loaded into the DIFFRAC.SUITE TOPAS® software and the peaks were identified and then indexed. In the indexing range, each of the crystal structures were systematically checked and in each one the space groups with a higher goodness of fit (Gof) were selected and their lattice parameters were noted. This process was repeated three times in

order to ensure reproducibility of the results. The best fitted space groups with their lattice parameters are shown in the **Table 4.2**. These are the results from the last repetition of the indexing process. The other two tables are in the **Appendix**, and there was not significant variation between each subsequent attempt.

Crystal structure	Space group	Gof	a (Å)	b (Å)	c (Å)
Cubic	Pa-3	3.67	24.495	24.495	24.495
Trigonal	P31	3.35	14.944	14.944	15.955
Tetragonal	P4bm	4.37	14.958	14.958	6.529
	I41/a	4.14	14.953	14.953	13.038
	P41212	4.14	14.958	14.958	6.529
	P42212	4.10	14.958	14.958	6.529
	I41	4.10	14.953	14.953	13.066
	I41/a	3.90	14.953	14.953	13.066
Orthorhombic	P222	4.21	18.424	12.642	5.092
	P2221	3.62	10.546	10.574	6.532
	P222	3.46	6.502	10.539	10.572
	P2221	3.45	10.521	6.537	10.610
Monoclinic	P2	4.67	10.280	10.589	5.628
	P2	4.72	12.475	10.635	5.597
	P2	4.37	11.023	10.613	5.589
Triclinic	P-1	4.20	4.994	7.558	13.386
	P-1	4.86	6.697	8.055	12.735

Table 4.2: The best space groups fits found during the peak indexing process.

Once the peak indexing was done, these best fitting space groups were fitted to the powder XRD pattern using a Pawley fit. In order to do this, a separate *hkl* phase was added in TOPAS for each space group, and each space group and its lattice parameters were introduced and refined one by one.

In this Pawley fit the better fits were the ones with the lowest Gof. The fitting process was repeated three times for all the space groups in order to provide some idea of reproducibility of the fitting results. The results obtained the first two times are in the **Appendix**. The results from the last round of fitting are represented in the **Table 4.3**.

Crystal structure	Space group	Gof	a(Å)	b(Å)	c(Å)
Cubic	Pa-3	14.12	24.541	24.541	24.541
Trigonal	P31	13.63	14.762	14.762	15.822
Tetragonal	P4bm	9.67	15.097	15.097	6.579
	I41/a	16.26	15.098	15.098	13.130
	P41212	9.75	15.098	15.098	6.580
	P42212	9.70	15.097	15.097	6.579
	I41	9.89	15.093	15.093	13.148
	I41/a	16.26	15.097	15.097	13.129
Orthorhombic	P222	10.14	18.519	12.663	5.103
	P2221	7.35	10.636	10.739	6.566
	P222	7.34	6.567	10.637	10.739
	P2221	7.34	10.637	6.567	10.739
Monoclinic	P2	8.46	10.770	10.658	5.608
	P2	20.25	12.439	10.657	5.598
	P2	8.51	10.738	10.635	5.589
Triclinic	P-1	12.51	5.0915	7.553	13.489
	P-1	13.36	6.856	8.235	12.941

Table 4.3: Results obtained after the Pawley fit of each space group in different crystal structures. The value of the lattice parameters changed from the initial indexing process in order to allow a better fit to the powder diffractogram.

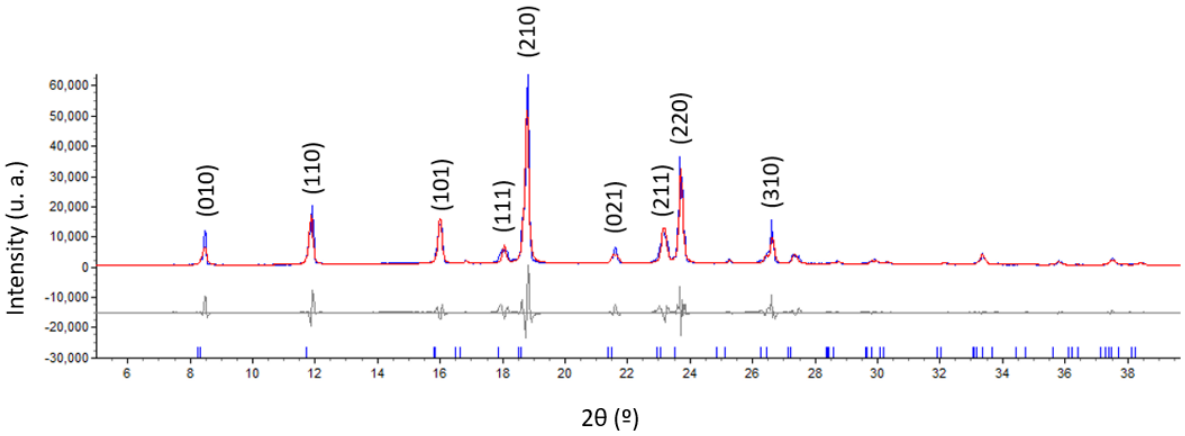

Figure 4.9: Comparison between the Pawley fit refinement and the powder diffractogram data.

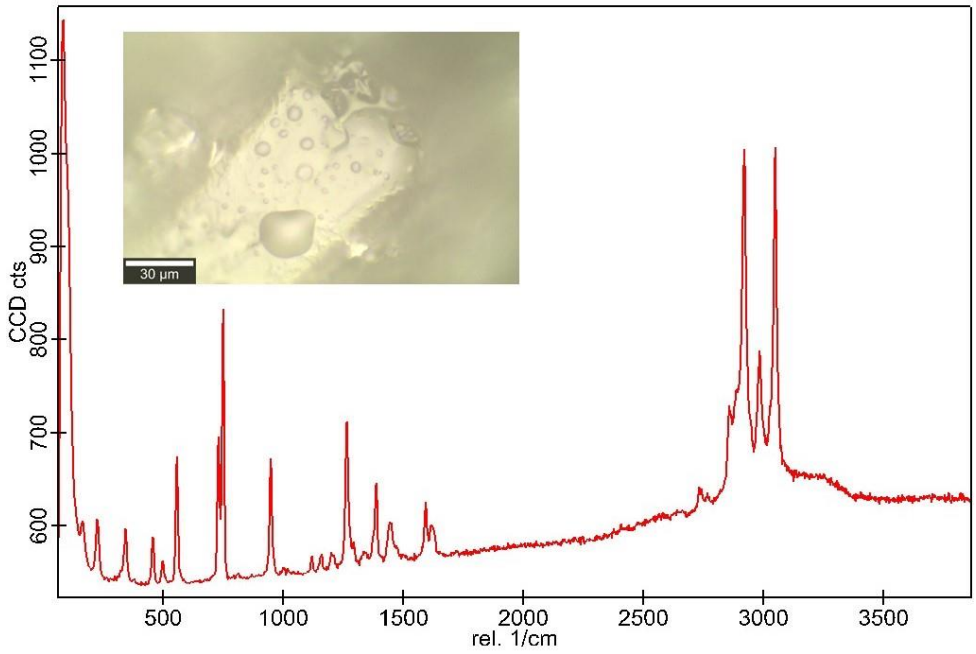

Figure 4.10: Raman analysis of *June 2022 crystals*.

In **Figure 4.10**, several peaks are shown which represent the structure of the material. According to the literature, the bands located at lower frequencies correspond to the inorganic compound and the ones located at higher frequencies are from the organic compound. [29,30]

4.3.3 Crystallization attempt 1

Since the obtained material was more of a gel than crystals, no XRD measurement was performed.

4.3.4 Crystallization attempt 2

Then, more analyses were done with the new synthetized materials. From *Crystallization attempt 2*, the white long-needle crystals were separated from the brownish ones, and both were analyzed. The brownish ones were still a bit wet even though they were left in the fume hood several days for letting them dry and its diffractogram did not have intense peaks.

However, the white crystals were analyzed and showed similar data as in **Figure 4.11**. These results have the same peak position as the other sample, but there is a lot of difference in the relative intensities compared with the crystals made in June.

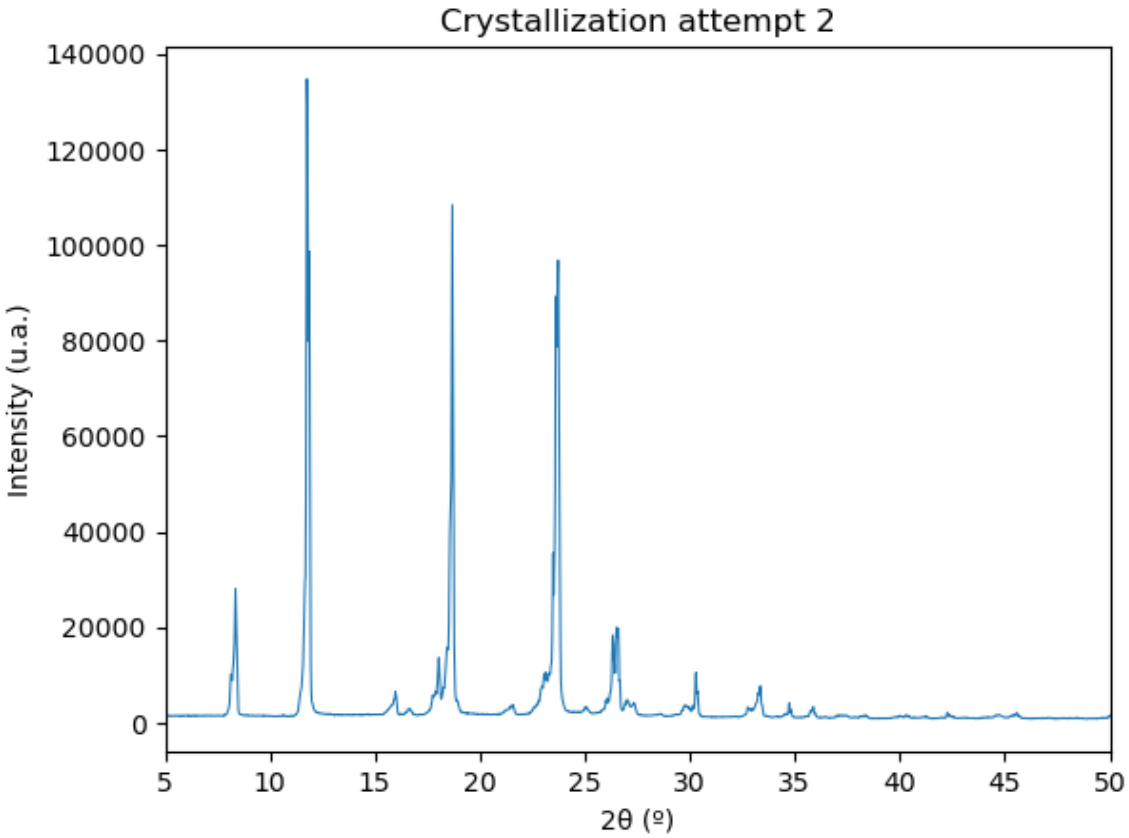

Figure 4.11: X-ray diffractogram of the white long-needle crystals made in the second synthesis attempt (*Crystallization attempt 2*).

For assuring that this new synthetized material was the same as the one made in June, a Pawley fit of the diffractogram was carried out. The structure and the lattice parameters used were the ones obtained after the structure determination of *June 2022 crystals* in the section **4.3.2**.

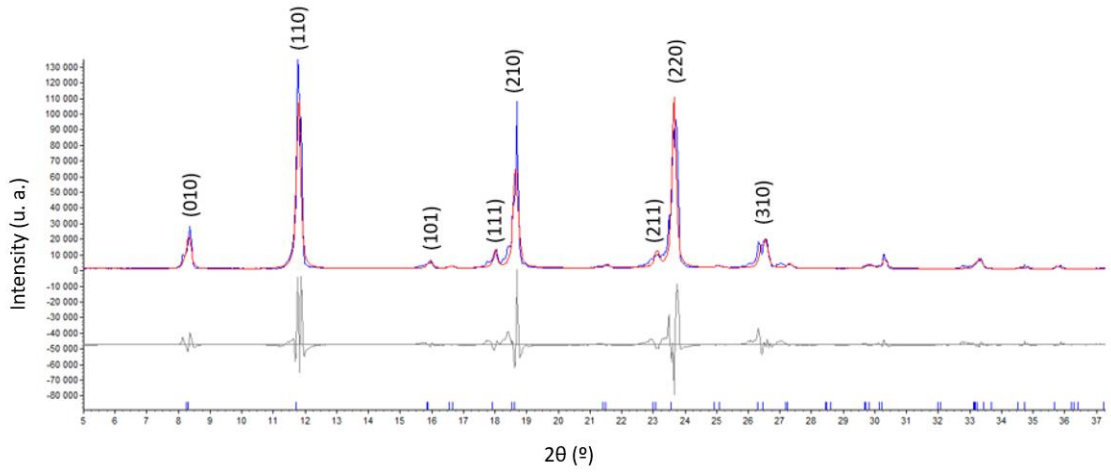

Figure 4.12: Comparison between the Pawley fit refinement and the powder diffractogram data.

After the Pawley fit with the orthorhombic system and the $P222_1$ space group, the lattice parameters were a=10.637 Å, b=10.711 Å, c=6.553 Å with a Gof of 16.01.

4.3.5 Crystallization attempt 3

The last diffractogram made was from the latest sample synthetized this semester. This time, the peaks were less intense with respect to the background. There was also a hump in the background observed between 2θ 15º and 35º.

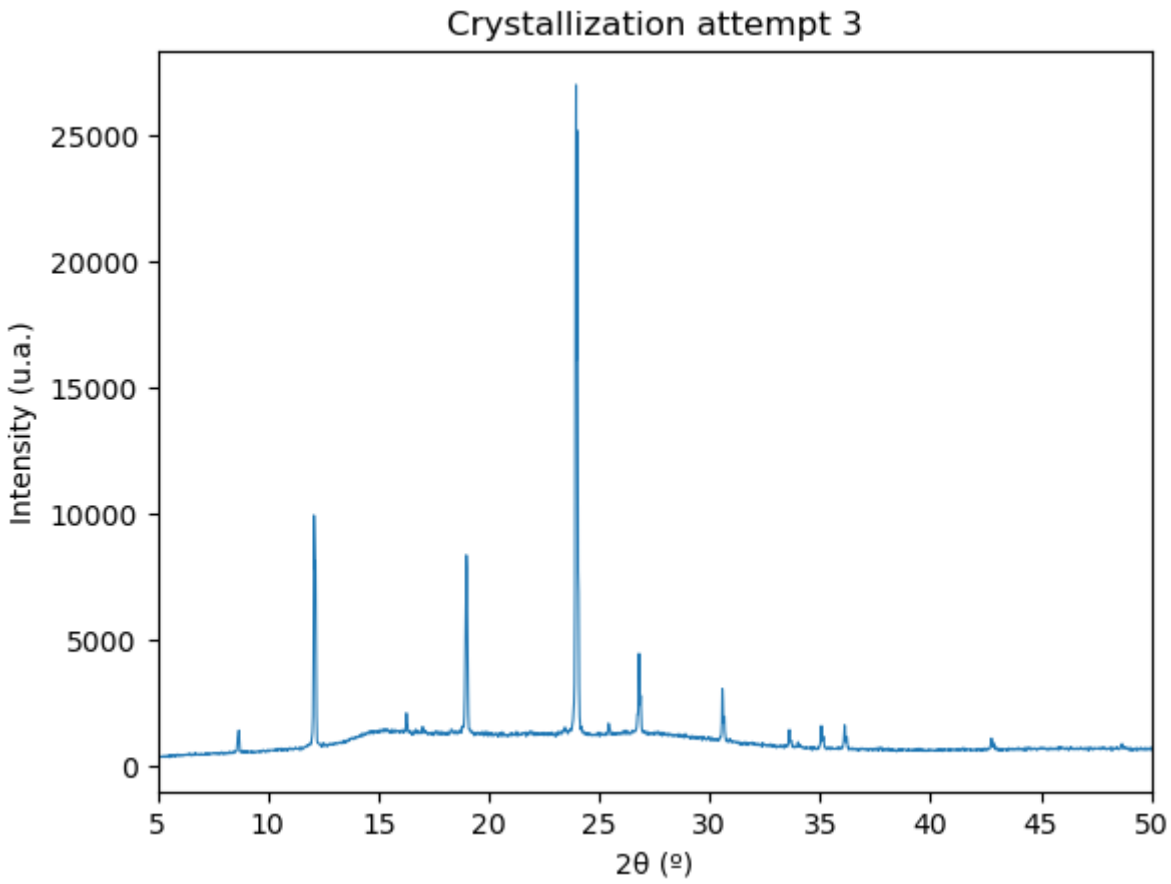

Figure 4.13: X-ray diffractogram of the *Crystallization attempt 3 crystals*.

As in *Crystallization attempt 2*, the data of the diffractogram of this material was Pawley fitted so it can be assured that the new synthetized material has the same structure as the crystals synthetized in June 2022.

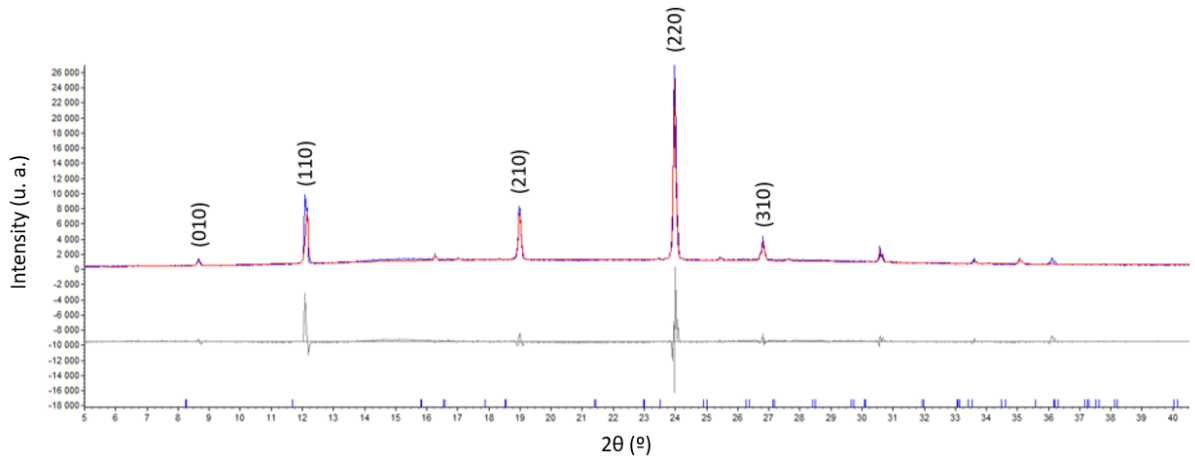

Figure 4.14: Comparison between the Pawley fit refinement and the powder diffractogram data.

The lattice parameters after the Pawley fit were a=10.675 Å, b=10.721 Å and c=6.566 Å, with a Gof of 4.21.

4.3.6 Crystallization attempt 4

This sample was not analyzed with X-ray diffraction.

4.3.7 Crystallization attempt 5

This sample was not analyzed with X-ray diffraction.

4.3.8 Structural stability as a function of thermal treatment

The structure of the $(DMP)_2$ $[ZnBr_2Cl_2]$ was observed to be stable at room temperature, with stability observed for periods of over 12 months. However, the fact that the transition temperature on cooling was just below room temperature (21°C) created an opportunity to study the transition ex situ (i.e. after thermal cycling). A study of the cooling rate was thus conducted to observe the effect this had on the crystal structure.

Two samples of $(DMP)_2$ $[ZnBr_2Cl_2]$ were melted by heating to 80 ºC and holding for 30 minutes in an oven at ambient pressure. Each sample was then cooled down under different conditions. One of the samples was removed from the oven to ambient conditions and allowed to cool naturally in a desiccator. The second sample was removed from the oven and placed immediately in a freezer at -18 ºC so that the sample was quenched. After 30 minutes it was then placed in a desiccator at room temperature (RT).

X-Ray analyses were carried out on both samples as a function of time after their return to room temperature. For scheduling reasons, the exact same intervals were not used for both samples. The diffractograms showing the results from the study are shown below.

Air-cooled sample

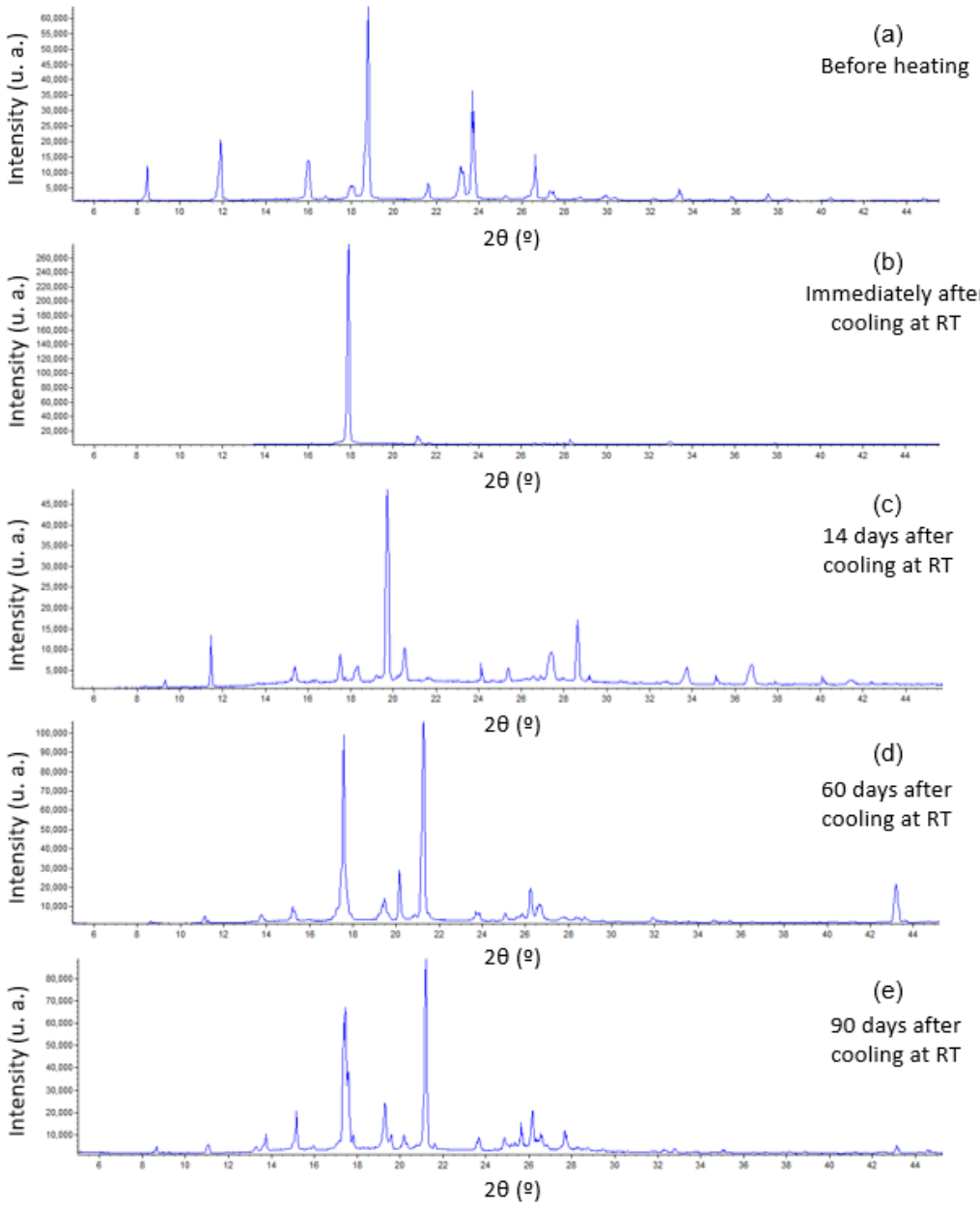

Figure 4.15: Diffractograms of the air-cooled sample. XRD powder diffractograms of intensity vs 2θ for $(DMP)_2$ $[ZnBr_2Cl_2]$ heated and cooled in ambient conditions. Each panel shows the $(DMP)_2$ $[ZnBr_2Cl_2]$ at a different time with respect to the heating cycle. (a) Before heating. (b) Immediately after cooling to room temperature. (c) 14 days after cooling. (d) 60 days after cooling. (e) 90 days after cooling.

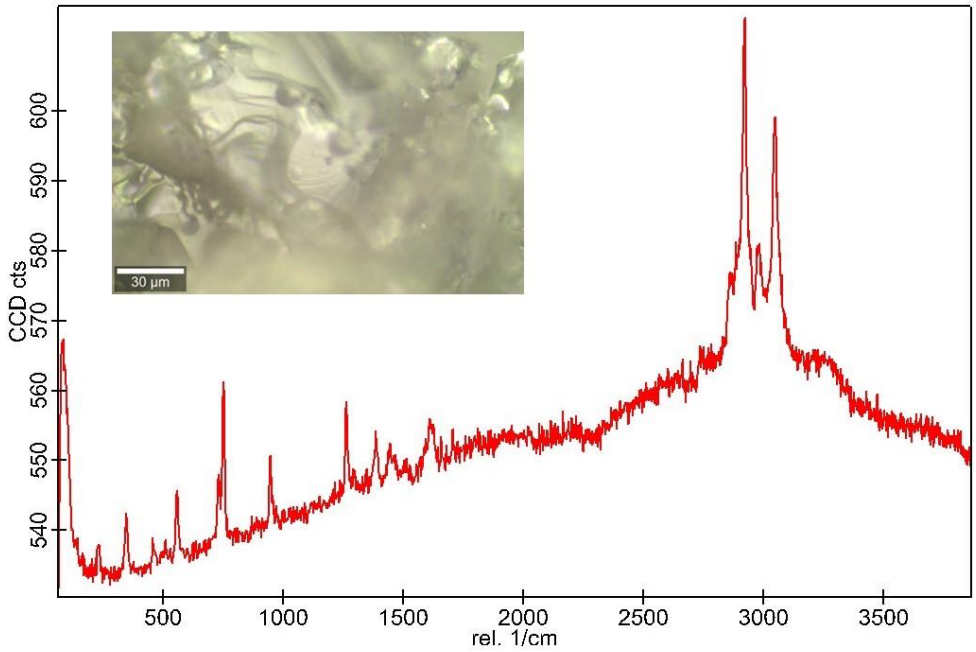

Figure 4.16: Raman analysis of the air-cooled sample.

The bands present in **Figure 4.16** are the same for the *June 2022 crystals*.

Quenched sample

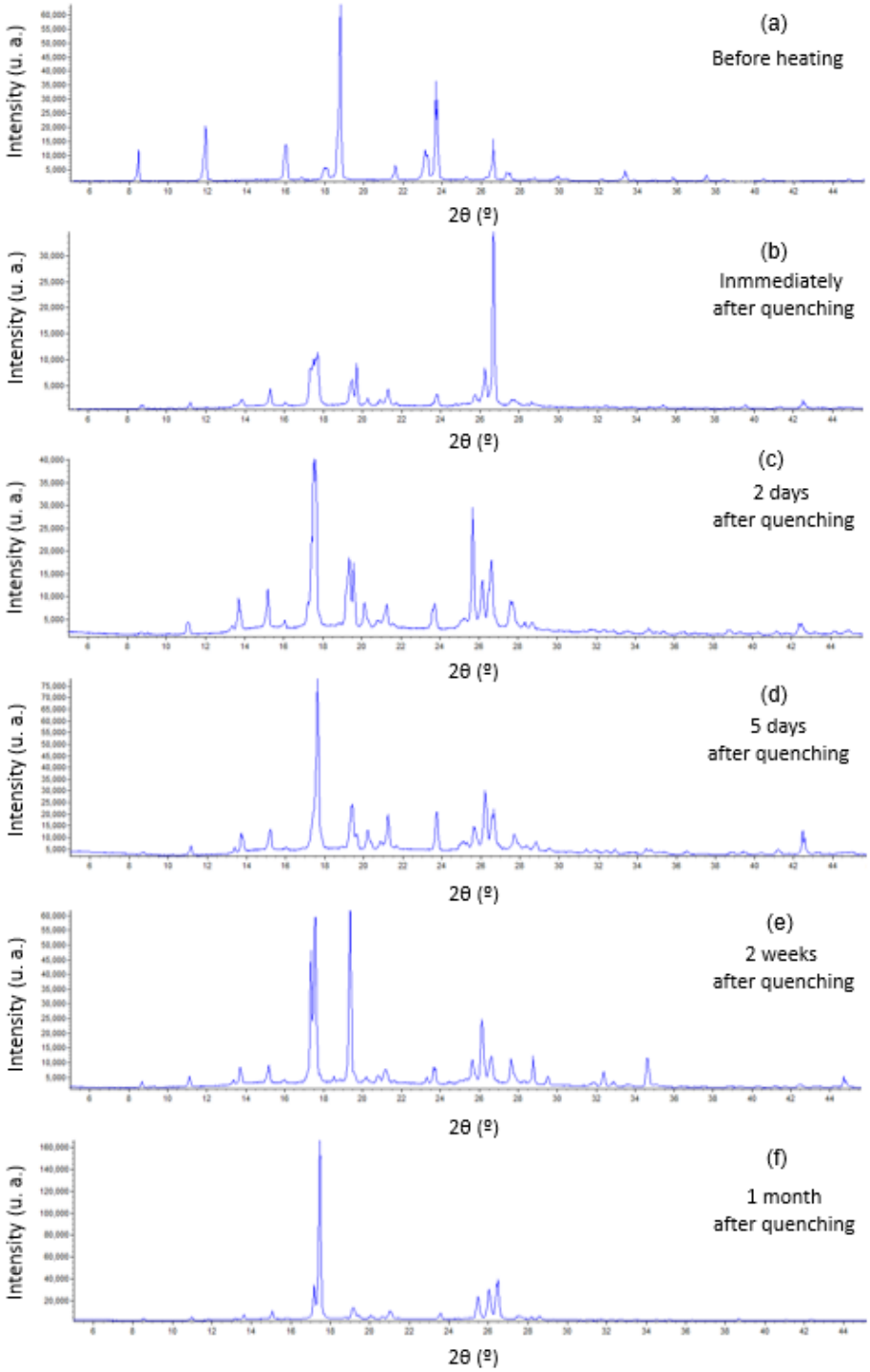

Figure 4.17. Diffractograms of the quenched sample. XRD powder diffractograms of intensity vs 2θ for $(DMP)_2$ $[ZnBr_2Cl_2]$and quenched at -18 ºC. Each panel shows the $(DMP)_2$ $[ZnBr_2Cl_2]$ at a different time with respect to the thermal treatment. (a) Before heating. (b) Immediately after quenching at -18 ºC. (c) 2 days after quenching. (d) 5 days after quenching. (e) 2 weeks after quenching. (f) 1 month after quenching.

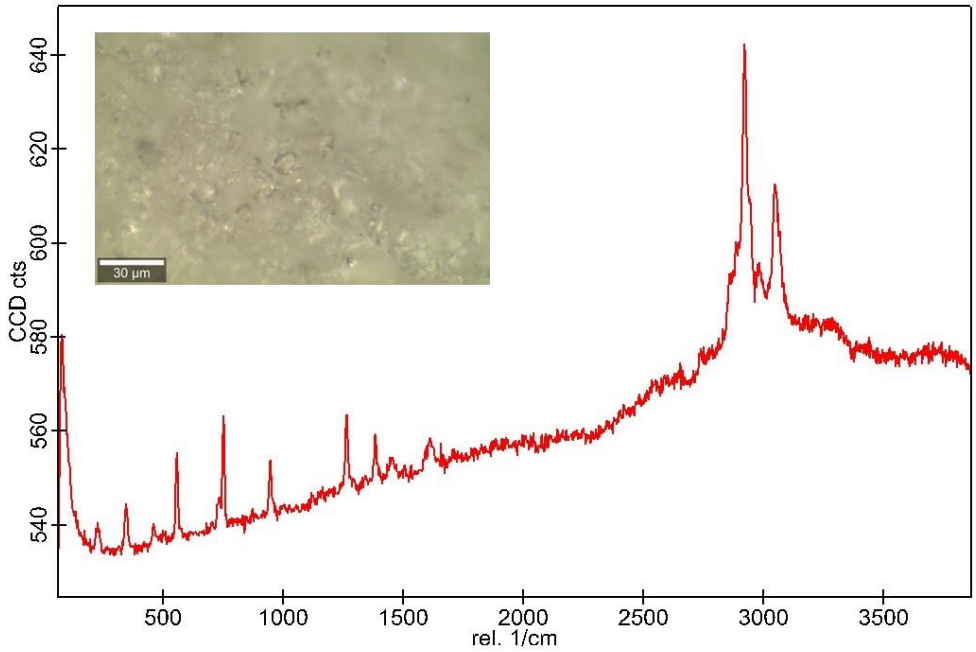

Figure 4.18: Raman analysis of the quenched sample.

The bands present in **Figure 4.16** are the same for the *June 2022 crystals*.

4.4 Phase transitions

For studying the phase transitions of the material, the *June 2022 crystals* were used. The previous students did an analysis the last semester of those crystals but with a different maximum a minimum temperature than the ones mentioned in the **section 3.3.1**. The maximum temperature of this analysis was 80 ºC and the minimum was -25 ºC.

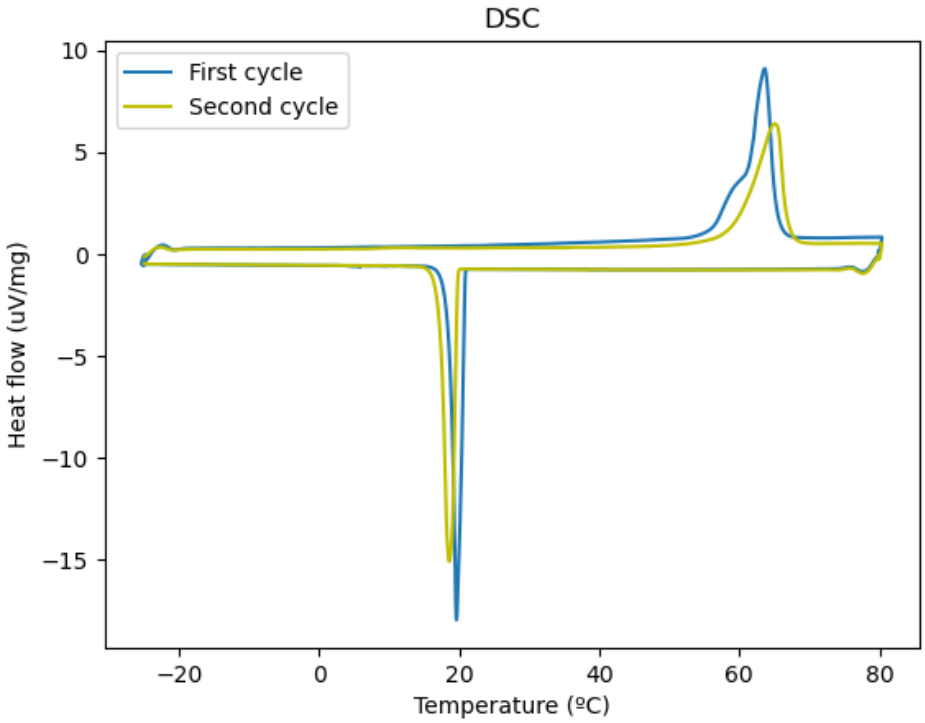

Figure 4.19: DSC analysis carried out by previous students in the last semester of the *June 2022 crystals*.

There are two transitions observed during the thermal cycle. The transition on heating occurs at 56 ºC, where all the energy is absorbed in an endothermic process, and the cooling one at 22 ºC, where the energy is released in an exothermic process. There is a hysteresis of 34 ºC between these two transitions. The enthalpy in the endothermic process has a value of 402.6 µVs/mg and in the exothermic transition 299.2 µVs/mg are released.

Another thermal analysis was carried out from -20 to 80 ºC, in which the material showed reversibility and reproducibility, since both endothermic and exothermic transitions were visible in each cycle.

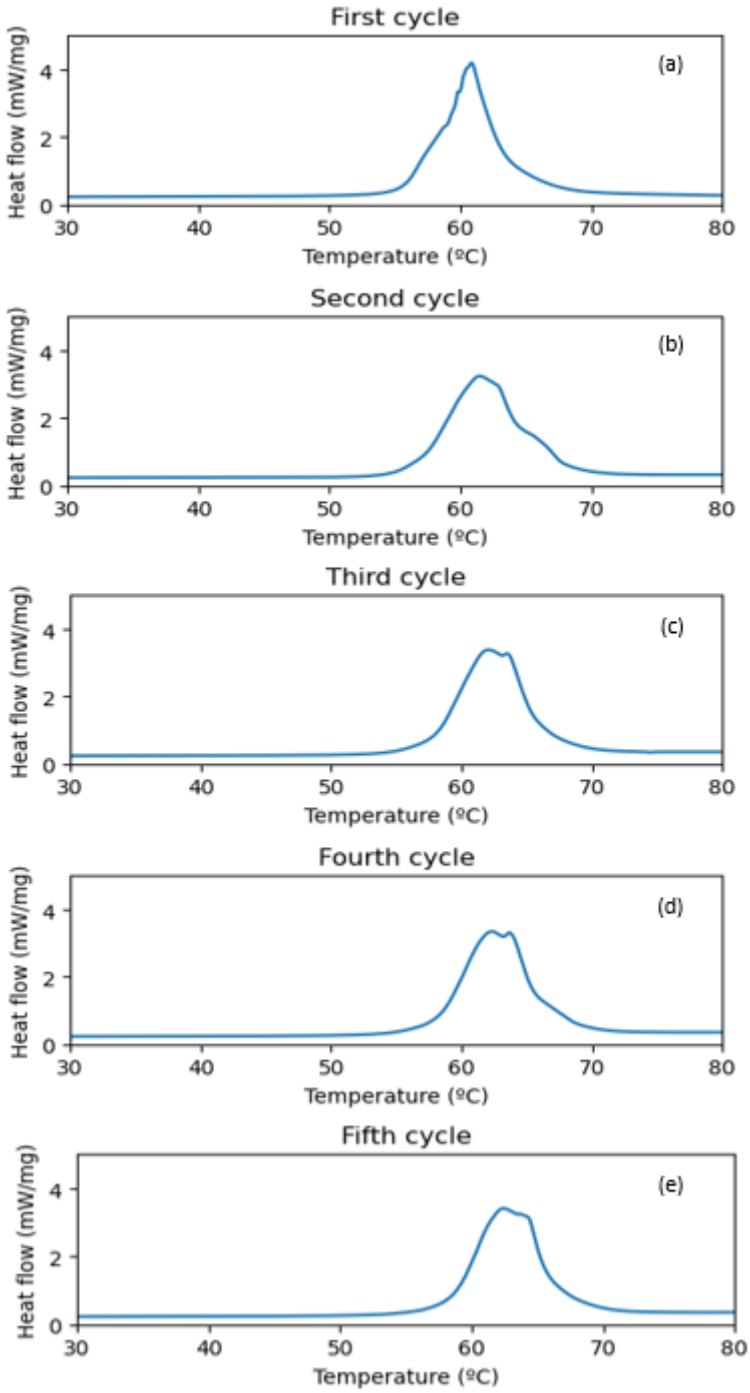

Figure 4.20: Evolution of the phase transition over multiple thermal cycles studied by DSC analysis for *June 2022 crystals*. Plots show heat flow as a function of temperature between 30 and 80 ºC during the heating cycle. The endothermic transitions of (a) first cycle, (b) second cycle, (c) third cycle, (d) fourth cycle and (e) fifth cycle, are represented. Due to instrument malfunction during cooling, the exothermic transition data were not accurate, so it is not shown in the figure.

Cycle	T_{melt} (ºC)	ΔH (J/g)
First	54.9	123.3
Second	53.6	118.3
Third	55.1	108.9
Fourth	53.4	113.2
Fifth	54.8	113.2

Table 4.4: Melting temperatures and enthalpies of the endothermic transitions of each cycle in the thermal analysis with a minimum temperature of -20 ºC and a maximum temperature of 80 ºC.

A further measurement was performed with a minimum temperature of -20 ºC and a maximum temperature of 75 ºC in the first cycle which was increased 5 ºC with every cycle until reaching 100 ºC.

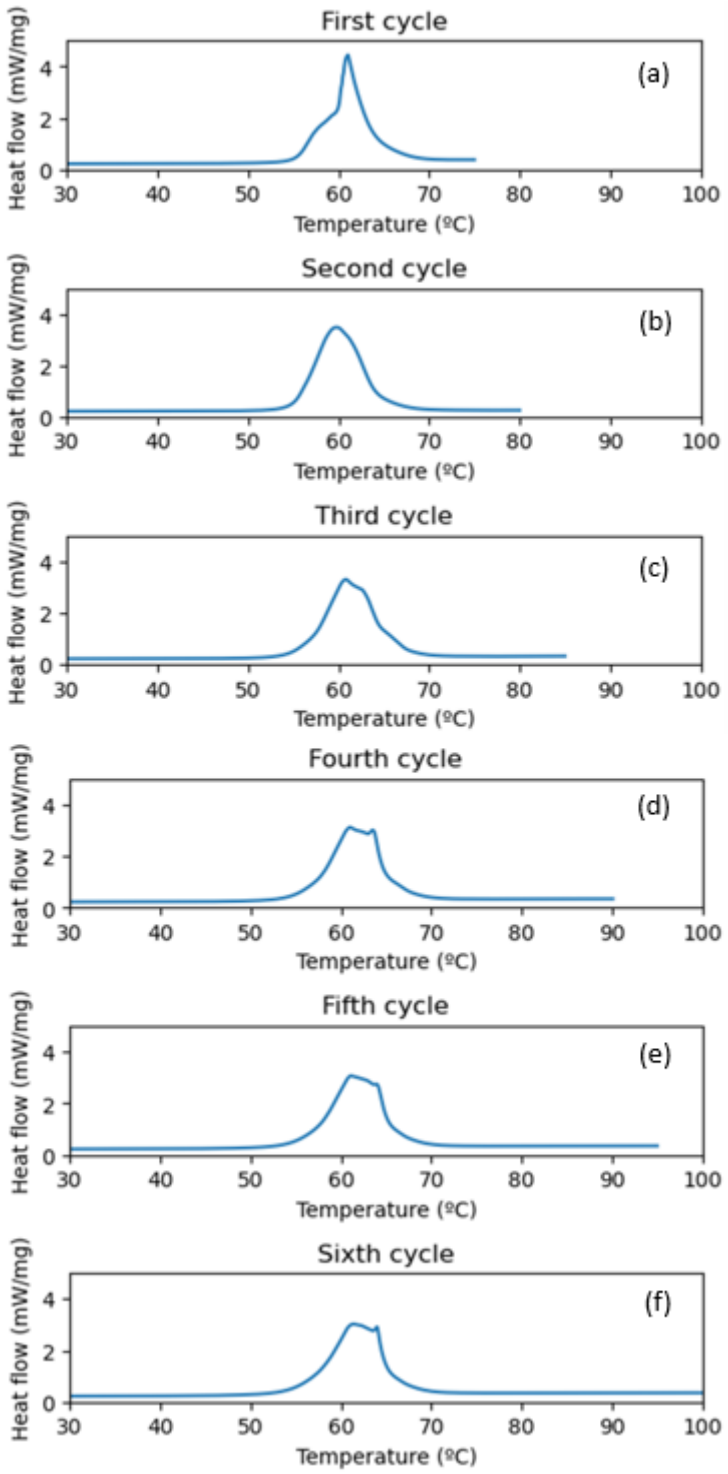

Figure 4.21: Evolution of the phase transition over multiple thermal cycles studied by DSC analysis for *June 2022 crystals*. Plots show heat flow as a function of temperature between 30 and 100 ºC during the heating cycle. (a) First cycle, (b) second cycle, (c) third cycle, (d) fourth cycle, (e) fifth cycle and (f) sixth cycle. Due to cooling malfunction on equipment the cooling cycles could not be analyzed.

Cycle	T_{melt} (ºC)	ΔH (J/g)
First	54.9	126.7
Second	54.1	122.6
Third	54.6	115.1
Fourth	53.4	116.1
Fifth	53.5	113.5
Sixth	53.9	116.1

Table 4.5: Melting temperatures and enthalpies of the endothermic transitions of each cycle in the thermal analysis with a minimum temperature of -20 ºC and a maximum temperature of 75 ºC which increases 5 ºC with each cycle until it reaches 100 ºC.

5 Discussion

5.1 Synthesis observations

5.1.1 Crystallization attempt 1

There was some crystallization that looks to be metastable, and when dried out, it redissolved, leaving the gel form, it could also be that the material is hygroscopic. So, because there was no crystal growth, the nucleation must have been suppressed, and because crystallization and nucleation are associated with the interaction of charge molecules, and the crystals are ionic, maybe there was no proper charge and the embryos could not properly, leading to no nucleation and subsequently to no growth, resulting in the amorphous material. The protonation process is problematic and maybe it went old because the cation precursor was a bit old and may have absorbed some moisture from the air, which may impact how the protonation happens.
The origin of the reddish crystals was unknown but could have been related to contamination with the Al or dissolved Br^- ions.

5.1.2 Crystallization attempt 2

The crystals were growing out of the walls and the temperature of evaporation was higher in the other attempts. The reason of that type of growth is that in the vicinity of the walls, the dissolution forms a meniscus, which is a curve in the surface of a molecular substance when it touches another material. When the solvent in the surface of the dissolution is evaporated, the concentration of the sample is locally higher than in the rest of the dissolution, but as the solvent molecules are in continuous movement, new solvent molecules quickly arrive from within the solution and the concentrations are homogenized. Since the solvent molecules' access to the meniscus portion is more restricted this procedure is more challenging there. As a result, there is a larger local concentration of solute there than in the rest of the solution, which causes that region to be where the solid crystallizes first.

At the bottom of the beaker, brownish crystals precipitated, and this is a cause of an error in the crystallization procedure. The solutions were totally evaporated instead of being purified first, so both the sample (with a white color) and impurities precipitated, and that is why the discoloration of the sample is present.

On the walls, there was a planar growth, because the shape of the crystals was in a needle shape, which is like an elongated prism, and can only be obtained with planar growth. This needle shape can be associated with an acicular crystal habit.

5.1.3 Crystallization attempt 3

These crystals are related more to a homogenous crystallization (although it is still heterogeneous since nothing is perfectly homogeneous), and the solution was growing from the bottom because the beaker was evaporating at room temperature, which is lower than the temperature used in the previous attempts, so the molecules in the solution were not evaporated as much this time. A small modification of the synthesis approach changed the result of the synthesis, that is how it crystallized at the bottom and the growth was more stable this time, since it was more isotropic.

These crystals are more like a tabular crystal habit, and the discoloration is still present because of the mistake in the evaporation process, as explained before in **section 5.1.2**.

5.1.4 Crystallization attempt 4

These crystals were white at the beginning of the crystallization, but once they were left longer in the fume hood for drying completely, they turned brown. This is because the sample was not correctly purified before letting it dry and the impurities precipitate with the material.

5.1.5 Crystallization attempt 5

These crystals did not turn into a brownish color, because before letting the solution dry, it was purified by filtration with a Kitasato flask by separating the mother liquors with the impurities from the sample. For this reason, this is the correct crystallization method and the obtained compound is the desired one.

5.2 Crystal structure

5.2.1 Crystallization attempt 2

The results of **Figure 4.11** compared to the ones from **Figure 4.8** show that the peaks have the same position in both, but their relative intensities change. This difference is likely related to the highly orientated crystal growth and the crystal habits because the needle-like growth occurs in one direction and it was expected to have different ratios of crystallographic direction, which

changes the intensity. After the Pawley fit, the Gof was 16.01, not really low, which indicates that the structures are similar but not completely the same. It could probably be because only the long white crystals which were attached to the walls of the beaker were analyzed, and the brownish crystals at the bottom of the beaker were set aside.

5.2.2 Crystallization attempt 3

In this last diffractogram (**Figure 4.13**), there are not additional peaks so there is not a crystalline secondary phase that is seen, but there is a lower peak intensity and a higher background. Since the intensity of the peaks from the diffractograms *of June 2022 crystals* and *Crystallization attempt 2* is higher, it can be said that there is a less crystalline phase and the hump of the background shows that there is more amorphous material. The brownish color can be related to an amorphous phase or uncrystallized material remaining.

The reason of the color can probably be related with the age of the precursors and the fact that they may have hydrated by bonding with OH^- coming from moisture. Before the protonation, the precursors were not properly dehydrated, so maybe the same degree of protonation in the *June 2022 crystals* is not achieved in the *Crystallization attempts 1*, *2* and *3*.

Even though there was discoloration in this sample, the structure is almost the same as the one determined from *June 2022 crystals*, since after the Pawley fit the Gof obtained was 4.21, which is low and indicates that it was a good fit.

5.3 Determination of the crystal structure

Looking at the Gof of each crystal structure, the better fits (shown in **Table 4.3**) are found in the orthorhombic system, and the chosen space groups for the structure of the material was $P222_1$ with a=10.636 Å, b=10.739 Å, c=6.566 Å as lattice parameters. However, two of the three lattice parameters of these systems have always a similar value, so the structure is quite close to a tetragonal structure if it were to be approximated or simplified. Even so, the orthorhombic systems had the lowest Gof, and it makes sense because in the orthorhombic systems one more degree of freedom is added, and it allows the system to fit better to the diffractogram.

5.3.1 Structural stability as a function of thermal treatment

Air-cooled sample

Figure 4.15a shows the structure of the material before it was heated. The powder diffraction pattern shows major peaks at 9, 12, 16, 19, 24 and 25 º 2θ with other minor reflections and is indicative of a single-phase material with the orthorhombic $P222_1$ crystal structure. This structure fitting is described previously in the thesis.

Figure 4.15b shows the structure at room temperature, after heating and cooling to room temperature. Only one major peak is visible at 18º 2θ with a few additional minor peaks present. While not directly comparable, it is noted that the intensity of the peaks was significantly higher than those found in other structural phases of this material. This type of diffractogram with only a few high intensity peaks is characteristic of the mesophase structures observed in plastic crystals. [5] These phases are related to the high degrees of molecular orientational disorder, which is explained in the introduction section of the thesis. This structure was determined as previously stated in the thesis, and it mostly belongs to a tetragonal system with a P42/n space group with a= 13.799 Å, b = 13.799 Å and c = 17.641 Å as lattice parameters (**Figure A.5)**.

The structural pattern observed in **Figure 4.15b** raises some interesting questions about the material when combined with other experimental observations. Firstly, we note that the material has only one first order phase transition visible between 25 and 80 ºC. Secondly, the material was observed to melt at this transition. The combination of these two facts suggests that the material does not form a mesophase on heating, but instead it has a solid to liquid transition consistent with standard crystalline materials. [31]

The XRD data immediately after cooling however, indicates the presence of a mesophase. When we again consider the DSC data (figure), which shows that the large hysteresis of the transition causes the transition temperature on cooling to be 21 ºC, i.e., right at room temperature, this indicates that the diffractogram after heating may in fact capture the material during the solidification transition, before the transition is complete. If this is true, it would mean that the mesophase is accessible as a metastable phase of the solidification process.

This phase was probably obtained because the phase transition temperature is right at room temperature, around 22 ºC, and an intermediate stage of the phase transition process was captured. There is not enough kinetic energy to continue quickly so it is progressing slowly.

The diffractogram in **Figure 4.15c** was obtained 2 weeks after the sample was heated. It is most notable that the diffraction pattern resembles neither the original room temperature pattern nor

the mesophase pattern captured immediately after cooling. Firstly, this indicates that the mesophase must be metastable, as the structure changes from the mesophase structure with time. However, as the structure does not return to the original room temperature structure there must be some additional influential factors. After trying to determine the structure of this sample, the most possible one resulted to be orthorhombic F222, with a=20.576 Å, b=27.518 Å, c=18.974 Å as lattice parameters (**Figure A.6**).

One hypothesis is that the organic molecules changes during heating. This may be likely as the 3,4-dimethylphenol has an oxygen atom which likes to bond with H forming a hydrate. It is thus likely that the molecule has a high affinity to moisture which may change the charge of the molecule and stability of the structure.

Another one could be that the inorganic anion is the one that changes when the samples are heated. It can condense with others and begin to form different structures. [32]

Figures 4.15d and **4.15e** represent the structures after 2 and 3 months respectively. Both are similar, which indicates that the materials structure eventually stabilizes with time, however, there is a significant difference between diffractograms at 2 weeks (**Figure 4.15c**) and 2 months (**Figure 4.15d**). While the underlying cause for this change is unknown the behavior generally fits with a kind of structural relaxation taking place slowly over time but with a more rapid changes happening in the period immediately following cooling. This could fit approximately with the kinetics of structural relaxation in system with constrained dynamics. [33] The structure for the sample after 2 months belongs to a monoclinic system with P21 as space group and a=14.452 Å, b= 20.440 Å and c=6.518 Å as lattice parameters (**Figure A.7**). The structure for the sample after 3 months belongs to a monoclinic system, with P2 as space group and a=23.113 Å b=12.907 Å and c=13.708 Å as lattice parameters (**Figure A.8**).

Quenched sample

Figure 4.17 represents a plot of the different diffractograms obtained from this sample. The **Figure 4.17a** represents the structure of the material before it was heated. This was the same material as used for the ambient cooling experiment and thus the structures of **Figure 4.15a** and **Figure 4.17a** are the same.

Figure 4.17b shows the powder diffraction pattern of the material at room temperature, immediately after being quenched to -18 ºC and then being allowed to return to room temperature. The XRD powder pattern of the quenched structure is distinctly different from the mesophase structure in **Figure 4.15b**, this is seen by the multiple peaks present and the lack of

the major high intensity mesophase peak at 18º 2θ. The structure that was determined for this material is from a hexagonal structure and P61 as space group, with a= 20.453 Å, b= 20.453 Å, and c=48.0522 Å as lattice parameters (**Figure A.9**).

However, there is a lower intensity peak in this vicinity, thus we are currently unable to rule out phase coexistence between the mesophase and another structure. The material was driven quickly through the one known phase transition observed with DSC by quenching, which further suggests that the mesophase structure is an intermediate phase state thermally stabilized by slow kinetics during a slow cooling process.

The room temperature structure after quenching however has lower peak intensities and fewer peaks, compared to the structure before heating, indicating that the structure may have less crystalline order. If this is the case, it may be explained by a freezing of the molecule orientational disorder due to the quenching process. Such behavior is seen in the literature in similar materials and is often referred to as reordering frustration or orientational glass phases. However, this is just a plausible hypothesis to explain the XRD observations, but further work is required to confirm.

Figure 4.17c shows the diffraction pattern of the structure after two days in the desiccator. The pattern shows a general increase in the peak intensities, with the peaks appearing sharper and more well defined and with the appearance of some new peaks, compared to that from the structure immediately after quenching (**Figure 4.17b**). While the intensities are not directly comparable between measurements, their increase relative to the background suggests that the degree of crystallinity of the material may have continued to increase with time at room temperature, indicating that if there was orientational disorder frozen into the structure due to quenching, then it is also metastable and relaxes as a function of time. This indicates relaxation of the quenched disorder at room temperature. One of the most probable structures of this sample was determined to belong a orthorhombic crystal structure with $C222_1$ as space group and a=18.409 Å, b=21.175 Å and c=32.643 Å as lattice parameters (**Figure A.10**).

Figure 4.17d shows the structure of the material after five days. The diffraction pattern is similar to the pattern after 2 days (**Figure 4.17c**) but many of the peaks again have higher intensities with respect to the background, which indicates that the relaxation process is continuing. Even though the intensity of the peaks is changing, the positions are the same, so the structure does not change. The hypothesis is that the structure is not fully crystalline after quenching, and it is slowly relaxing to a fully ordered structure. The structure that is more likely

to belong to this sample, is from an orthorhombic system, with Pmc21 as the space group, and a=17.606 Å, b=27.588 Å and c=13.968 Å as lattice parameters (**Figure A.11**).

Figure 4.17e represents the structure after two weeks. The pattern is similar to the one after 2 days with some further intensity change and a notable peak splitting present at approximately 18º 2θ. This indicates that the structure is still changing, although it appears that the crystal system and symmetry remains constant. The slight changes however indicate that there is still relaxation and perhaps some structural instability. The structure determined for this sample is monoclinic P2, with a=17.695 Å, b=10.278 Å and c=14.831 Å as lattice parameters (**Figure A.12**).

Figure 4.17f shows the structure 1 month after quenching. There is significant difference between this powder diffraction pattern and the one taken after two weeks (**Figure 4.17e**). the main peak appearing at 18º 2θ has a much high intensity than the other peaks. The other less intense peaks appear to match up with positions of peaks seen in **Figure 4.17e**. This change is unexpected as it does not indicate an increased structural stability and slowed relaxation with time, as was seen with the structure after ambient cooling. At this point in time, we have no explanation for this behavior, although it may be possible that the structural stability is affected by the humidity of the laboratory, which is not controlled.

From both data sets the main conclusion is that the crystal structure after the material has been melted is less stable than the structure after crystallization. This indicates that the thermal cycling is less stable than the structure after crystallization and that the structure obtained from the melt is not as stable as the structure grown during crystallization from solution precipitation. The changes of the structure in each study might be caused by the by organic cation, which possesses an oxonium group, coming from the protonation of an alcohol by an acid. Because they have a positive charge, protonated alcohols are significantly more reactive toward nucleophiles than neutral alcohols. [34]

Figure 5.1: Protonation of an alcohol by an acid which produces an oxonium ion.

The relaxed structure of the quenched material is possibly from a monoclinic or triclinic system. However, the monoclinic with C2 as space group and a=19.5655611 Å, b=13.048461 Å, c=18.5732793 Å and β=115.3134 º as lattice parameters was chosen because it has a low Gof and the range of the lattice parameters is similar to the ones from the original structure, whereas the triclinic system and P-1 space group has higher lattice parameters and since does not impose any symmetry conditions on the structure (**Figure A.13**).

A Pawley fit of this C2 monoclinic structure was done to the relaxed air-cooled sample, and the Gof after doing it was 11.07, which is quite high. This means that there is a poor correlation between the structures because they relax differently. It cannot be known if this difference comes from the heat treatment conditions or if it just not reproducible and the structures change over time because the material is being degraded. A repetition of the same experiment but with different conditions would be needed for proving this.

It can also be seen from this study that there is a mesophase on cooling but not on quenching. The mesophase state is not thermodynamically stable in this material, but it is kinetically stabilized on air cooling as the transition is not allowed to complete due to the temperature stopping at the transition temperature (22 ºC).

5.3.2 Raman spectroscopy

This analysis was performed in order to check if there was something affecting the structure and its stability. Water was thought to be the cause of the instability but since the characteristic water bands did not appear, which are located at 3355 and 3583 cm^{-1}, for two OH bands, [35] the compounds seem to not have absorbed any moisture during the thermal cycle that they were suppressed under. In the region of 200 and 300 cm^{-1} the bands from Zn-Cl and Zn-Br appear. A band at 200 cm^{-1} is visible and due to its high intensity, it could come from a combination of both Zn-Cl and Zn-Br, indicating that the condensation process could take place. [32]

5.4 Phase transitions

In DSC analyses, there are different phase transitions where the material can absorb or release energy. In the transitions that absorbs energy, occurs an endothermic process, and when it is released, there is an exothermic process.

As seen as in the **Figure 4.19**, the material has a phase transition when the energy is absorbed at 56 ºC and this energy is later released at 22 ºC. These transitions are reversible, so the material

can store and release energy in more than one cycle, and there is a hysteresis of 34 ºC, which is important because depending on this hysteresis the material can be used for different applications, and because of its temperature range, it can be used for domestic applications in homes. It could not be applied for industry applications since it would need to have the transitions at higher temperatures.

In **Figure 4.20** and **Figure 4.21**, other DSC analyses are represented, which go from -20 to 80 ºC and -20 to 100 ºC respectively. Even though the exothermic transition that takes place while cooling was not represented, since the data was not accurate due to cooling malfunctioning of the instrument, it is proven that both phase transitions are reversible and stable, because the energy absorbed with each cycle is constant after several cycles.

Another analysis of *June 2022 crystals* was performed, but with a thermal profile that goes from 25 to 80 ºC.

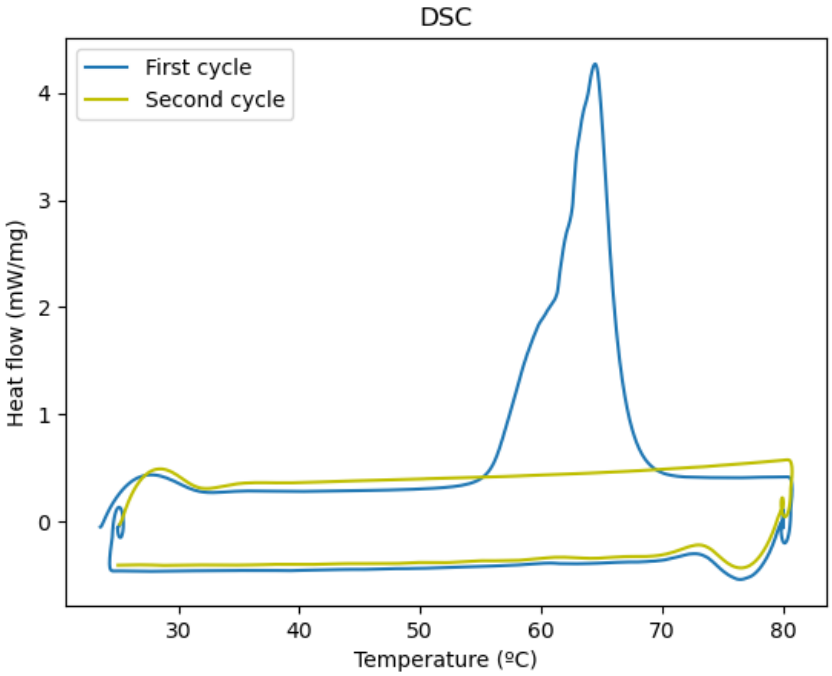

Figure 5.2: DSC analysis carried out of *June 2022 crystals*. The analysis has a thermal profile with a minimum temperature of 25 ºC and a maximum temperature of 80 ºC.

Only one phase transition can be seen, it occurs at 56 ºC, as in the previous made by the previous students. The cooling phase transition is not seen because the material was not cooled enough, so it stayed all the time in the same phase even in the second cycle of the analysis. The enthalpy of the phase transition in the **Figure 5.2** is 126.1 J/g, which is higher than the enthalpy of a commercial plastic crystal, which is around 100 J/g. [1]

This data supports the theory of **section 5.3.1**, that in the air-cooled sample, the material stops just before the transition, so the crystallization is slow and depending on the cooling temperature and the time of cooling, the phase transition will be visible or not. In addition, it proves that even if the material has a different crystal structure after heating or cooling, the transition appears to be reversible and is little effected by the exact crystal symmetry of the low temperature solid structure. That is partly why it was difficult to determine that the phase transition is likely a solid-liquid transition and not a solid-solid transition like originally thought.

6 Conclusion

Green energy future needs renewable energy, and since this cannot be used constantly, because sunlight and wind are not available always, this energy needs to be stored. Almost half of the energy used is in form of heat, so one viable option for storing energy is thermal energy storage. Plastic crystals are a new type of material which can store thermal energy and release it through phase transitions. They are solid-solid phase change materials which avoid leakage problems found in other solid-liquid materials, so they are easier to contain and thus have wider potential for application and device design. In addition, they can store more energy than other solid-solid materials, because they have a mesophase where the crystal structure is maintained and the molecules gain free energy through increased orientational freedom, increasing entropy and the amount of energy they can store. Due to their advantages, it is important to study plastic crystals and related molecular materials in order to gain insight and understand them better.

The material that has been studied in this project, $(DMP)_2$ $[ZnBr_2Cl_2]$, has never been characterized before, so there was no previous literature about it. Its structure has been determined, Orthorhombic $P222_1$ with a=10.636 Å, b=10.739 Å, c=6.566 Å as lattice parameters. However, the material ended up not being a plastic crystal since it did not show a solid-solid phase transition but a solid-liquid transition. Nevertheless, the capacity for storing thermal energy with this transition has been studied and it can store more energy than the average commercial plastic crystal with an enthalpy of transition of 126.1 J/g, and since the phase transitions occur around room temperature, it could be used in housing (domestic) thermal energy storage applications, such as, absorbing heat at times of the day when the temperatures are high and releasing the thermal energy at night when the temperatures lower, thus helping to regulate a comfortable indoor temperature throughout a daily cycle.

In addition, a structure study has been conducted in which the material has been subject to different thermal conditions after melting. This study revealed that a mesophase occurs as part of the transition from liquid to solid and is thermally stabilized by holding the temperature in the middle of the transition. The sample quenched to below room temperature showed that it is not possible (under the conditions tested) to kinetically stabilize the mesophase by freezing in the orientational disorder by rapid cooling.

Bibliography

(1) Fallahi, A.; Guldentops, G.; Tao, M.; Granados-Focil, S.; Van Dessel, S. Review on Solid-Solid Phase Change Materials for Thermal Energy Storage: Molecular Structure and Thermal Properties. *Applied Thermal Engineering*. Elsevier Ltd 2017, pp 1427–1441. https://doi.org/10.1016/j.applthermaleng.2017.08.161.

(2) Dincer, I.; Dost, S.; Li, X. Performance Analyses of Sensible Heat Storage Systems for Thermal Applications. *Int J Energy Res* **1997**, *21*, 1157–1171.

(3) Khadiran, T.; Hussein, M. Z.; Zainal, Z.; Rusli, R. Advanced Energy Storage Materials for Building Applications and Their Thermal Performance Characterization: A Review. *Renewable and Sustainable Energy Reviews*. Elsevier Ltd May 1, 2016, pp 916–928. https://doi.org/10.1016/j.rser.2015.12.081.

(4) Timmermans, J. Plastic Crystals: A Historical Review. *Journal of Physics and Chemistry of solids* **1961**, *18*, 1–8.

(5) Walker, J.; Marshall, K. P.; Salgado-Beceiro, J.; Williamson, B. A. D.; Løndal, N. S.; Castro-Garcia, S.; Andújar, M. S.; Selbach, S. M.; Chernyshov, D.; Einarsrud, M. A. Mesophase Transitions in [(C2H5)4N][FeBrCl3] and [(CH3)4N][FeBrCl3] Ferroic Plastic Crystals. *Chemistry of Materials* **2022**, *34* (6), 2585–2598. https://doi.org/10.1021/acs.chemmater.1c03778.

(6) Li, G. Sensible Heat Thermal Storage Energy and Exergy Performance Evaluations. *Renewable and Sustainable Energy Reviews*. Elsevier Ltd January 1, 2016, pp 897–923. https://doi.org/10.1016/j.rser.2015.09.006.

(7) Salgado Beceiro, J.; Socorro, D.; García, C.; Sánchez Andújar, M. *Hybrid Organic-Inorganic Materials with Phase Transitions for Solid-State Cooling and Solar Thermal Energy Storage Directors*.

(8) Pielichowska, K.; Pielichowski, K. Phase Change Materials for Thermal Energy Storage. *Progress in Materials Science*. Elsevier Ltd 2014, pp 67–123. https://doi.org/10.1016/j.pmatsci.2014.03.005.

(9) Faraj, K.; Khaled, M.; Faraj, J.; Hachem, F.; Castelain, C. Phase Change Material Thermal Energy Storage Systems for Cooling Applications in Buildings: A Review. *Renewable and Sustainable Energy Reviews* **2020**, *119*. https://doi.org/10.1016/j.rser.2019.109579.

(10) Singh, S. *Phase Transitions in Liquid Crystals*; 2000; Vol. 324. https://doi.org/https://doi.org/10.1016/S0370-1573(99)00049-6.

(11) Yang, T.; King, W. P.; Miljkovic, N. Phase Change Material-Based Thermal Energy Storage. *Cell Reports Physical Science*. Cell Press August 18, 2021. https://doi.org/10.1016/j.xcrp.2021.100540.

(12) Sarbu, I.; Sebarchievici, C. A Comprehensive Review of Thermal Energy Storage. *Sustainability (Switzerland)*. MDPI January 14, 2018. https://doi.org/10.3390/su10010191.

(13) Zalba, B.; Marín, J. M.; Cabeza, L. F.; Mehling, H. *Review on Thermal Energy Storage with Phase Change: Materials, Heat Transfer Analysis and Applications*. www.elsevier.com/locate/apthermeng.

(14) Timmermans, J. Un Nouvel État Mésomorphe: Les Cristaux Organiques Plastiques. *J. de Chim. Phys.* **1938**, *35*, 331–334.

(15) Dong, X. H.; Hsu, C. H.; Li, Y.; Liu, H.; Wang, J.; Huang, M.; Yue, K.; Sun, H. J.; Wang, C. L.; Yu, X.; Zhang, W. Bin; Lotz, B.; Cheng, S. Z. D. Supramolecular Crystals and Crystallization with Nanosized Motifs of Giant Molecules. *Advances in Polymer Science* **2017**, *276*, 183–214. https://doi.org/10.1007/12_2015_343.

(16) Harada, J. Plastic/Ferroelectric Molecular Crystals: Ferroelectric Performance in Bulk Polycrystalline Forms. *APL Materials*. American Institute of Physics Inc. February 1, 2021. https://doi.org/10.1063/5.0039066.

(17) Li, B.; Kawakita, Y.; Ohira-Kawamura, S.; Sugahara, T.; Wang, H.; Wang, J.; Chen, Y.; Kawaguchi, S. I.; Kawaguchi, S.; Ohara, K.; Li, K.; Yu, D.; Mole, R.; Hattori, T.; Kikuchi, T.; Yano, S. ichiro; Zhang, Z.; Zhang, Z.; Ren, W.; Lin, S.; Sakata, O.; Nakajima, K.; Zhang, Z. Colossal Barocaloric Effects in Plastic Crystals. *Nature* **2019**, *567* (7749), 506–510. https://doi.org/10.1038/s41586-019-1042-5.

(18) Lunkenheimer, P.; Michl, M.; Loidl, A. Nonlinear Dielectric Response of Plastic Crystals; 2018; pp 277–300. https://doi.org/10.1007/978-3-319-77574-6_9.

(19) Harada, J.; Yoneyama, N.; Yokokura, S.; Takahashi, Y.; Miura, A.; Kitamura, N.; Inabe, T. Ferroelectricity and Piezoelectricity in Free-Standing Polycrystalline Films of Plastic Crystals. *J Am Chem Soc* **2018**, *140* (1), 346–354. https://doi.org/10.1021/jacs.7b10539.

(20) Pringle, J. M.; Howlett, P. C.; MacFarlane, D. R.; Forsyth, M. Organic Ionic Plastic Crystals: Recent Advances. *J Mater Chem* **2010**, *20* (11), 2056–2062. https://doi.org/10.1039/b920406g.

(21) Boldrin, D. Fantastic Barocalorics and Where to Find Them. *Applied Physics Letters*. American Institute of Physics Inc. April 26, 2021. https://doi.org/10.1063/5.0046416.

(22) Askeland, D.; Fulay, P.; Wright, W. *Ciencia e Ingeniería de Materiales*, 6ª Edición.

(23) Yu, L.; Reutzel-Edens, S. M. *Encyclopedia of Food Sciences and Nutrition*, 2nd Edition.; 2003. https://doi.org/https://doi.org/10.1016/B0-12-227055-X/00313-8.

(24) Mullin, J. W. *Crystallization*, 4th Edition.; 2001.

(25) Berlin, S.-V.; Gmbh, H. *The Physics of Phase Transitions Physics and Astronomy*. http://www.springer.de/phys/.

(26) Anantharaman, T. R.; Suryanarayana, C. *Review: A Decade of Quenching from the Melt*; 1971; Vol. 6.

(27) Foulon, M.; Amoureux, J. P.; Sauvajol, J. L.; Lefebvre, J.; Descamps, M. *Evidence of a "glassy Crystal" Phase Obtained by the Quenching of the Plastic Phase of the Cyanoadamantane*; 1983; Vol. 16.

(28) Gardiner, D. J.; Graves, P. R. *Practical Raman Spectroscopy*; 1989.

(29) Green, J. H. S.; H~rison, D. J.; Kynaston, W. *Vibrational Spectra of Bemene Derivatives-XV !L!He Dimethylphenols, 2,6-, 2,53 and 3,44ichlorophenol*; 1970.

(30) Irish, D. E.; Mccarroll, B.; Young, T. F. Raman Study of Zinc Chloride Solutions. *J Chem Phys* **1963**, *39* (12), 3436–3444. https://doi.org/10.1063/1.1734212.

(31) Umeyama, D.; Horike, S.; Inukai, M.; Itakura, T.; Kitagawa, S. Reversible Solid-to-Liquid Phase Transition of Coordination Polymer Crystals. *J Am Chem Soc* **2015**, *137* (2), 864–870. https://doi.org/10.1021/ja511019u.

(32) Yannopoulos, S. N.; Kalampounias, A. G.; Chrissanthopoulos, A.; Papatheodorou, G. N. Temperature Induced Changes on the Structure and the Dynamics of the "Tetrahedral" Glasses and Melts of ZNCl2 and ZnBr2. *Journal of Chemical Physics* **2003**, *118* (7), 3197–3214. https://doi.org/10.1063/1.1537246.

(33) Avramov, I.; Tonchev, V. *Kinetics of Structural Relaxation in a Constrained Dynamics System*; 1996; Vol. 194.

(34) McMurry, J. *Organic Chemistry*, 3rd ed.; 1992.

(35) Ćorluka, V.; Hederić, Ž.; Hadžiselimović, M. *Moisture Measurement in Solid Samples Using Raman Spectroscopy*.

Appendix

Indexing results

Crystal structure	Space group	Gof	a (Å)	b (Å)	c (Å)
Tetragonal	P4/nbm	6.42	14.970	14.970	10.412
	P41	6.30	10.558	10.558	12.996
	P42cm	6.20	10.539	10.539	13.004
	P4	5.01	10.559	10.559	6.494
	P42	6.00	10.558	10.558	12.996
Orthorhombic	Cmc21	18.21	14.987	14.898	6.503
	C222	17.14	14.987	14.898	6.503
	Pbcn	15.76	14.984	14.874	6.504
	C2221	15.27	14.823	14.985	6.491
Monoclinic	Cc	308.91	15.544	5.926	10.607
	C2	216.24	15.544	5.926	10.607
	P21	89.89	12.834	7.513	10.267
	P21	86.43	12.834	7.513	10.267
Triclinic	P-1	1E+11	3.859	5.748	8.703

Table A.1: First results from the peak indexing.

Crystal structure	Space group	Gof	a (Å)	b (Å)	c (Å)
Cubic	P213	2.08	16.720	16.720	16.720
	Pa-3	2.08	16.779	16.779	16.779
	P23	2.00	16.779	16.779	16.779
	P4332	2.96	28.268	28.268	28.268
Trigonal-Hexagonal	P3c1	2.33	21.226	21.226	5.389
	P3	2.81	21.206	21.206	5.359
Tetragonal	P4	2.57	10.456	10.456	6.618
	P4	2.7	9.978	9.978	13.251
	P42	2.64	10.456	10.456	6.618
	P4cc	2.59	14.464	14.464	11.680
	P41	2.51	10.248	10.248	13.052
	P42cm	2.44	14.423	14.423	11.697
Orthorhombic	P222	3.67	16.458	10.043	10.509
	P222	3.07	10.535	12.966	9.9484
	P21212	3.56	16.504	10.515	10.065
	P2221	3.44	16.458	10.043	10.509
	Pmc21	3.33	9.958	10.503	12.956
	Pmc21	3.21	10.631	9.669	7.473
	Pmn21	3.28	10.631	9.669	7.473
	Pmn21	3.05	12.947	9.951	10.561
	Pca21	2.85	10.631	9.669	7.473
Monoclinic	P21	5.83	8.806	10.579	10.679
	P21	4.56	9.956	12.895	7.261
	P2	4.68	5.522	10.569	10.603
Triclinic	P-1	7.76	6.905	7.397	12.112

Table A.2: Second results from the peak indexing.

Pawley fitting

Crystal structure	Space group	Gof	a (Å)	b (Å)	c (Å)
Tetragonal	P4/nbm	12.69	14.993	14.993	10.401
	P41	8.74	10.651	10.651	13.121
	P42cm	8.67	10.652	10.652	13.119
	P4	9.66	10.675	10.675	6.578
	P42	8.75	10.651	10.651	13.121
Orthorhombic	Cmc21	8.33	15.065	14.979	6.541
	C222	8.42	15.056	14.966	6.537
	Pbcn	8.75	15.047	14.956	6.532
	C2221	8.35	14.971	15.059	6.538
Monoclinic	Cc	20.70	15.441	5.968	10.639
	C2	20.37	15.490	5.996	10.649
	P21	15.62	12.473	7.534	10.264
	P21	15.22	12.686	7.557	10.285
Triclinic	P-1	18.38	3.883	5.748	8.702

Table A.3: First results from the Pawley fitting.

Crystal structure	Space group	Gof	a (Å)	b (Å)	c (Å)
Cubic	P213	18.66	16.902	16.902	16.902
	Pa-3	18.42	16.905	16.905	16.905
	P23	18.69	16.880	16.880	16.880
	P4332	15.64	28.314	28.314	28.314
Trigonal-Hexagonal	P3c1	16.35	21.578	21.578	5.348
	P3	17.07	21.551	21.551	5.345
Tetragonal	P4	9.66	10.675	10.675	6.579
	P4	15.22	10.091	10.091	13.209
	P42	9.66	10.675	10.675	6.578
	P4cc	13.52	14.628	14.628	12.053
	P41	15.22	10.105	10.105	13.224
	P42cm	11.18	14.673	14.673	12.078
Orthorhombic	P222	8.57	16.437	10.082	10.498
	P222	9.66	10.524	12.929	9.929
	P21212	8.61	16.427	10.485	10.069
	P2221	8.57	16.435	10.080	10.496
	Pmc21	10.43	9.922	10.471	12.916
	Pmc21	16.19	10.610	9.667	7.472
	Pmn21	16.18	10.611	9.668	7.473
	Pmn21	9.33	12.921	9.920	10.565
	Pca21	16.42	10.622	9.681	7.474
Monoclinic	P21	13.92	8.741	10.634	10.684
	P21	11.13	9.892	12.883	7.180
	P2	8.46	5.590	10.636	10.737
Triclinic	P-1	17.01	6.905	7.259	12.165

Table A.4: Second results from the Pawley fitting.

Crystal structure	Space group	Gof	a (Å)	b (Å)	c (Å)
Cubic	Ia-3	10.03	39.517	39.517	39.517
	Ia-3	9.90	39.533	39.533	39.533
	Ia-3	9.91	39.554	39.554	39.554
	P4332	7.59	26.959	26.959	26.959
	P4332	7.30	27.031	27.031	27.031
Trigonal-Hexagonal	R3c	6.19	14.569	14.569	60.006
	R3c	6.27	14.589	14.589	60.172
	R3c	6.20	14.568	14.568	60.007
	R3	7.05	10.346	10.346	87.972
	R3	6.99	10.233	10.233	88.791
Tetragonal	P42/n	5.82	13.799	13.799	17.641
	I4	8.10	9.797	9.797	70.892
	I4	7.21	13.906	13.906	28.843
	I41/a	9.12	18.548	18.548	24.652
	P41	7.48	13.163	13.163	17.897
Orthorhombic	C222	7.26	8.512	6.074	65.265
	P212121	6.33	11.696	17.232	14.653
	C222	7.48	8.472	6.228	70.202
	P2221	6.97	10.550	17.188	13.679
	Pca21	6.33	17.140	18.798	5.351
Monoclinic	P2	6.03	18.867	6.100	11.986
	P2	7.18	19.959	13.368	5.429
	P2	7.72	17.300	4.916	10.367
	P2	6.66	21.863	4.935	10.114
	P21	6.03	18.869	6.101	11.987
Triclinic	P-1	6.25	6.789	5.518	37.871
	P-1	8.46	7.219	8.373	18.085
	P-1	6.04	6.144	7.322	24.111
	P-1	6.13	7.240	16.139	26.480
	P-1	6.15	7.369	10.752	18.506

Table A.5: Results of air-cooled sample immediately after cooling at room temperature.

Crystal structure	Space group	Gof	a (Å)	b (Å)	c(Å)
Cubic	Pa-3	11.64	30.608	30.608	30.608
	Pa-3	11.61	30.616	30.616	30.616
	Pa-3	11.64	30.614	30.614	30.614
	Pa-3	11.82	33.696	33.696	33.696
	I-43d	9.55	41.944	41.944	41.944
Trigonal-Hexagonal	R3	41.53	64.600	64.600	11.929
	R3	9.52	44.850	44.850	12.448
	R3	10.70	55.398	55.398	10.286
	R3c	9.21	64.632	64.632	11.944
	R3	9.69	16.342	16.342	128.266
	P31	10.45	20.855	20.855	23.229
Tetragonal	P4/n	8.35	10.355	10.355	68.817
	P4/n	10.52	7.697	7.697	74.090
	P4/n	9.40	10.452	10.452	57.536
	I41	9.79	14.255	14.255	111.868
	I41/a	10.09	16.219	16.219	96.440
	P4212	10.18	7.701	7.701	74.120
Orthorhombic	F222	6.66	20.582	27.532	18.992
	F222	6.66	18.984	20.579	27.527
	F222	6.63	20.576	27.518	18.974
	Ccc2	6.85	16.466	18.946	19.348
	Pba2	7.62	19.439	18.733	16.535
Monoclinic	P21	7.08	10.178	16.290	10.978
	P21	7.08	10.178	16.294	10.980
	P2	6.87	10.179	16.304	10.986
	P2	6.81	10.173	16.293	10.984
	Pc	8.18	10.382	13.259	13.656
Triclinic	P-1	6.67	8.565	11.023	19.751
	P-1	6.61	10.978	12.343	15.968
	P-1	6.44	10.907	12.035	17.388
	P-1	6.60	10.110	16.428	12.035
	P-1	6.81	7.531	13.049	20.555

Table A.6: Results of air-cooled sample 14 days after cooling at room temperature.

Crystal structure	Space group	Gof	a (Å)	b (Å)	c(Å)
Cubic	I23	25.67	39.017	39.017	39.017
	I23	24.70	39.159	39.159	39.159
	I23	24.70	39.159	39.159	39.159
	I4132	20.23	39.012	39.012	39.012
	I4132	20.24	39.012	39.012	39.012
Trigonal-Hexagonal	P3	21.62	13.503	13.503	21.431
	P3	21.64	13.508	13.508	21.444
	P3	21.81	13.467	13.467	21.359
	P61	20.84	31.679	31.679	7.000
	P3	21.75	13.485	13.485	21.456
Tetragonal	P42212	10.91	18.584	18.584	24.389
	P42212	10.91	18.584	18.584	24.389
	P4212	10.49	18.582	18.582	24.388
	I41	12.51	11.897	11.897	91.509
	I41	19.60	12.665	12.665	92.926
Orthorhombic	C2221	10.00	38.483	8.944	20.425
	P21212	11.09	14.656	13.883	12.805
	C222	10.02	38.483	8.944	20.425
	Pba2	9.84	20.420	13.537	10.887
Monoclinic	P21	8.80	14.452	20.440	6.518
	P2	8.81	14.450	20.438	6.516
	C2	10.86	67.118	4.290	6.473
	C2	11.01	63.689	4.289	6.472
	C2	11.01	63.689	4.289	6.472
Triclinic	P-1	9.20	10.624	13.323	9.000
	P-1	9.86	10.681	12.878	8.996
	P-1	8.73	10.650	11.286	11.416
	P-1	14.72	7.439	12.055	16.343
	P-1	8.53	6.815	16.281	21.381

Table A.7: Results of air-cooled sample 60 days after cooling at room temperature.

Crystal structure	Space group	Gof	a (Å)	b (Å)	c(Å)
Cubic	Fd-3	22.18	55.523	55.523	55.523
	F4132	14.60	55.536	55.536	55.536
	Fd-3	22.11	55.542	55.542	55.542
	F23	25.06	55.539	55.539	55.539
	F4132	14.66	55.543	55.543	55.543
Trigonal-Hexagonal	P3	15.76	11.657	11.657	76.070
	P61	11.25	11.657	11.657	76.063
	P31	15.60	11.658	11.658	76.069
	P63	11.28	11.657	11.657	76.060
	P3 (tri)	15.83	11.888	11.888	50.936
Tetragonal	P4	13.19	14.561	14.561	50.934
	P4/n	13.60	13.096	13.096	82.082
	I41/amd	11.35	13.041	13.041	82.340
	I4	16.26	13.074	13.074	81.561
	P42212	10.77	14.565	14.565	50.946
Orthorhombic	C222	13.49	25.306	6.072	51.721
	C222	10.53	27.738	5.689	71.242
	C222	11.34	8.970	9.197	90.154
	C222	11.79	20.451	4.254	50.636
	C222	11.86	9.147	9.423	63.979
Monoclinic	Cc	11.36	91.691	12.877	6.492
	P2	14.77	11.854	10.405	27.169
	P2	12.47	23.154	12.907	13.708
	P21	12.84	23.113	12.889	13.686
	C2	9.56	155.981	14.359	12.518
Triclinic	P-1	10.31	11.402	15.448	26.306
	P-1	13.46	10.885	25.974	26.904
	P-1	8.68	9.531	17.449	13.127
	P-1	12.67	14.469	31.624	26.878
	P-1	11.42	9.454	15.512	26.744

Table A.8: Results of air-cooled sample 90 days after cooling at room temperature.

Crystal structure	Space group	Gof	a (Å)	b (Å)	c (Å)
Cubic	Pa-3	13.29	36.909	36.909	36.909
	I4132	8.78	52.133	52.133	52.133
	I23	7.82	52.064	52.064	52.064
	I4132	8.73	52.144	52.144	52.144
	Pn-3n	8.76	40.411	40.411	40.411
	P213	10.66	32.849	32.849	32.849
Trigonal-Hexagonal	P61	6.16	11.940	11.940	97.432
	P61	6.16	20.453	20.453	48.052
	P61	6.98	20.387	20.387	47.799
	P64	6.83	20.397	20.397	47.820
	R3	6.74	13.127	13.127	95.437
	P63	7.52	26.019	26.019	23.668
Tetragonal	P41	6.10	10.180	10.180	131.189
	P4	5.93	10.173	10.173	131.238
	P42/n	7.43	10.224	10.224	131.980
	P41212	5.36	10.225	10.225	132.001
	P42	5.61	10.156	10.156	131.251
	P41	5.56	10.160	10.160	131.309
Orthorhombic	C2221	6.60	57.313	35.814	5.304
	C222	6.61	57.365	35.845	5.311
	F222	6.99	25.790	32.975	18.287
	I222	5.42	62.942	10.776	17.259
	F222	6.96	25.754	18.275	32.957
	P222	5.96	49.737	10.256	8.645
Monoclinic	Pc	5.63	12.622	50.813	9.289
	C2	6.93	54.645	11.034	16.810
	Cc	25.65	21.806	28.310	29.234
	P21	9.12	17.572	6.354	16.803
	P2	9.16	17.567	6.351	16.799
	P21	9.25	17.560	6.328	16.782
Triclinic	P-1	5.09	6.640	15.662	16.961
	P-1	4.31	6.534	15.729	20.911
	P-1	11.70	6.638	17.827	25.133

Table A.9: Results of quenched sample immediately after quenching.

Crystal structure	Space group	Gof	a (Å)	b (Å)	c (Å)
Cubic	Ia-3	6.07	55.586	55.586	55.586
	Ia-3d	9.25	55.587	55.587	55.587
	Ia-3	6.10	55.572	55.572	55.572
	Fd-3	10.94	66.592	66.592	66.592
	Pa-3	10.50	30.749	30.749	30.749
Trigonal-Hexagonal	R3c	10.63	41.471	41.471	34.148
	R3	10.04	26.139	26.139	48.223
	R3	10.36	24.391	24.391	32.592
	P3	9.79	10.618	10.618	90.492
	R3	10.68	24.394	24.394	32.596
Tetragonal	P4/n	7.57	10.100	10.100	87.843
	P4bm	7.94	21.127	21.127	23.799
	P4/n	7.64	10.112	10.112	87.997
	P4	7.70	10.109	10.109	87.952
	P4	8.01	12.791	12.791	41.096
Orthorhombic	Cmc21	6.35	18.383	21.147	32.614
	C2221	5.85	18.409	21.175	32.643
	I222	9.26	40.980	25.606	10.479
	F222	8.35	25.255	15.025	48.656
	Ccca	6.88	17.753	12.220	128.303
	F222	8.37	25.290	48.658	15.002
Monoclinic	Pc	10.63	10.004	37.370	10.296
	P21/c	9.39	14.554	24.953	12.099
	P21	11.53	9.656	32.820	13.612
	P21	9.63	18.034	9.645	14.642
	P2	12.11	12.258	12.826	20.090
	C2	6.39	13.848	34.861	16.775
Triclinic	P-1	6.50	10.676	13.728	13.860
	P-1	6.73	16.410	10.859	21.768
	P-1	6.11	10.678	13.426	13.879
	P-1	6.19	13.918	9.630	13.660

Table A.10: Results of quenched sample 2 days after quenching.

Crystal structure	Space group	Gof	a (Å)	b (Å)	c (Å)
Cubic	I-43d	11.60	50.078	50.078	50.078
	P4332	9.46	38.702	38.702	38.702
	P23	17.46	38.698	38.698	38.698
	P213	17.73	38.697	38.697	38.697
	P23	17.36	38.697	38.697	38.697
	P213	17.77	38.700	38.700	38.700
Trigonal-Hexagonal	P3	14.53	11.212	11.212	71.701
	P63	14.20	10.382	10.382	104.134
	P63	9.27	13.137	13.137	70.935
	P3	15.27	10.237	10.237	104.107
	P6cc	9.14	19.994	19.994	31.799
	P3	14.53	11.212	11.212	71.701
	R3	9.74	21.147	21.147	62.366
Tetragonal	I4	18.95	17.493	17.493	106.437
	P4	10.18	10.190	10.190	88.614
	P4	10.05	10.124	10.124	88.228
	P4/n	9.96	10.139	10.139	88.310
	I4	9.03	18.436	18.436	62.244
Orthorhombic	I222	7.03	18.518	61.569	9.356
	Ima2	7.60	18.453	61.453	9.324
	I222	7.51	18.368	61.981	9.424
	Abm2	6.74	19.415	9.289	83.663
	C2221	8.32	25.780	9.497	66.778
	P222	10.35	16.131	17.629	13.356
	Pmc21	8.94	17.606	27.588	13.968
Monoclinic	C2	8.02	69.393	13.514	11.090
	P2	10.81	10.142	17.621	16.015
	C2	8.89	20.684	9.461	17.813
	C2	8.91	20.682	9.462	17.815
Triclinic	P-1	6.89	8.059	12.462	33.305
	P-1	10.57	9.696	16.767	32.352
	P-1	8.33	8.648	20.574	26.957
	P-1	7.76	9.481	11.459	43.896

Table A.11: Results of quenched sample 5 days after quenching.

Crystal structure	Space group	Gof	a (Å)	b (Å)	c (Å)
Cubic	Pa-3	11.56	41.389	41.389	41.389
	Pa-3	11.75	41.454	41.454	41.454
	Pn-3	11.66	41.474	41.474	41.474
	P23	14.01	31.052	31.052	31.052
Trigonal-Hexagonal	P31c	19.09	25.739	25.739	24.305
	P61	10.42	26.000	26.000	24.456
	P31	77.39	26.005	26.005	24.461
	P3	220.33	25.896	25.896	24.305
	P3	13.74	11.899	11.899	66.027
Tetragonal	I41md	5.96	18.919	18.919	95.322
	P42/n	15.43	12.137	12.137	112.751
	I4	5.73	18.328	18.328	143.649
	I4	10.96	18.273	18.273	65.454
	P4	20.01	14.277	14.277	71.898
Orthorhombic	Cmc21	6.63	12.387	13.153	102.049
	Ima2	13.49	48.011	22.685	6.038
	P21212	7.51	50.775	8.571	10.322
	I222	9.19	48.296	22.976	6.102
	Pcca	13.37	17.580	23.990	14.536
Monoclinic	P2	5.61	17.695	10.278	14.831
	P21	11.76	18.451	4.922	19.486
	P2	11.76	18.452	4.922	19.487
	P2	10.78	23.772	14.071	13.162
	P21	8.00	27.678	7.283	10.569
Triclinic	P-1	6.26	9.803	10.482	20.323
	P-1	5.61	9.132	23.873	26.531
	P-1	6.46	12.017	23.894	13.651
	P-1	6.43	9.558	13.632	22.316
	P-1	6.44	8.171	14.446	21.949

Table A.12: Results of quenched sample 2 weeks after quenching.

Crystal structure	Space group	Gof	a (Å)	b (Å)	c (Å)
Cubic	Pa-3	19.86	40.254	40.254	40.254
	P-43n	13.56	40.134	40.134	40.134
	P4332	11.37	30.138	30.138	30.138
	P213	14.00	30.138	30.138	30.138
	Pn-3	13.23	30.138	30.138	30.138
Trigonal-Hexagonal	P3	12.80	12.248	12.248	58.401
	P3	21.55	13.631	13.631	69.441
	P31	12.44	12.242	12.242	58.314
	P31	11.67	12.219	12.219	58.922
Tetragonal	P4/n	9.02	10.368	10.368	105.799
	P4212	8.19	14.598	14.598	48.739
	I4cm	8.51	23.980	23.980	38.320
	P4	10.30	14.616	14.616	53.633
	P4	9.91	10.366	10.366	53.327
	P4	10.25	10.161	10.161	81.758
Orthorhombic	Abm2	9.17	41.054	6.810	65.664
	C222	9.14	20.831	8.958	52.830
	C222	9.04	21.407	8.892	58.105
	Abm2	7.82	41.886	3.602	58.843
	P222	10.45	50.243	10.503	7.122
	C2221	10.69	20.978	9.459	50.916
Monoclinic	P2	9.45	11.973	10.663	22.515
	P21	9.47	11.972	10.661	22.512
	C2	6.84	19.566	13.048	18.573
	C2	7.46	19.495	12.857	18.327
Triclinic	P-1	11.05	15.963	28.231	21.502
	P-1	9.03	12.891	27.076	30.262
	P-1	6.30	10.481	22.618	18.177
	P-1	9.37	11.443	15.812	21.365

Table A.13: Results of quenched sample 1 month after quenching.